# Improving the Representation of Hydrological Processes by the Multi-dimensional Modeling Approach

Ying Zhao[1,2,*], Jun Yi[3], Rongjiang Yao[4], Fei Li[5], Robert Lee Hill[6]

*[1]College of Resources and Environmental Engineering, Ludong University, Yantai 264025, China; [2]Department of Ecosystem Science and Management, Pennsylvania State University, University Park, PA 16802, USA; [3]Hubei Province Key Laboratory for Geographical Process Analysis and Simulation, Central China Normal University, Wuhan 430079, China; [4]State Key Laboratory of Soil and Sustainable Agriculture, Institute of Soil Science, Chinese Academy of Sciences, Nanjing 210008, China; [5]Grassland Research Institute, Chinese Academy of Agricultural Sciences, Huhhot 010010, China; [6]Department of Environmental Science and Technology, University of Maryland, College Park, MD 20742, USA.*

*[*]Corresponding author: yzhaosoils@gmail.com (Y. Zhao)*

**Abstract:** Watershed hydrological processes controlled by subsurface structures that have hierarchical organization across scales, but there is a lack in multiscale model validation. In this study, using a comprehensive dataset collected in the forested Shale Hills catchment, we tested the series HYDRUS codes (i.e., HYDRUS-1D at the pedon scale, HYDRUS-2D at the hillslope scale, and HYDRUS-3D at the catchment scale) that included a hierarchical multi-dimensional modeling approach for water flow simulation in the vadose zone. There is good agreement between 1D simulations and measurements of soil moisture profiles controlled by soil hydraulic parameters and precipitation characteristics; however, short-term fluctuations in preferential flow were poorly captured. Notably, 2D and 3D simulations (Nash–Sutcliffe efficiency, *NSE >0.5*), which accounting subsurface preferential flow controlled by slope positions and shallow fractured bedrock, provided better results than 1D simulations (*NSE <0.5*). Our modeling approach also illustrated that the studied watershed was characterized by weathered and un-weathered fracture bedrocks, which routed water through a network of subsurface preferential flow pathways to the first-order stream. Furthermore, a dual-porosity or anisotropy model produced more accurate predictions than a single-porosity or isotropy model due to a more realistic representation of local soil characteristics and layered structure. Our multi-dimensional modeling approaches credited with diagnosing and presenting the dominant hydrological processes and the interactions within soil-landscape features across one sloped catchment.

Keywords: Hydrological processes; Subsurface preferential flow; Multi-dimensional Model; Fracture bedrock; HYDRUS

Soil is a three-dimensional structural unit that is subject to different preferential flow processes under varying precipitation inputs, soil-terrain attributes and moisture conditions. Preferential flow, defined by Hendrickx and Flury (2001) as 'all phenomena where water and solutes move along certain pathways, while bypassing a fraction of the porous matrix', results in irregular wetting patterns which water moves faster in certain parts of the soil profile than in others (Freeze, 1972). Understanding the dynamics of preferential flow is critical for the design of monitoring schemes and for formulating models (Lin and Zhou, 2008; Clark et al., 2015). In the early periods, hydrology was considered as one-dimensional vertical flow, neglecting the 3D (vertical + lateral) subsurface water flow (Fan et al., 2019). In order to increase the predictive capability of hydrology models, it is necessary to include phenomena such as fast transport through macropores, furrow flow due to the spatial variability of hydraulic properties, and fingering flow due to the instability of wetting fronts (Vogel and Roth, 2003; Vereecken et al., 2015; Gao et al., 2018).

Although preferential flow is ubiquitous in hydrology, it is still difficult to measure and quantify across space and time (Beven and Germann, 1982; Nimmo, 2012; Beven and Germann, 2013; Liu and Lin, 2015). Its proper identification and representation in hydrological models remain a challenge (Schulz et al., 2006; Beven and Germann, 2013; Clark et al., 2015; Gu et al., 2018). Onset of instability and preferential flow and their subsequent processes are intimately related to the spatial structure of the subsurface heterogeneities caused by biologic or geological activities as well as geomorphological and soil-forming processes. Current developments in geophysical (e.g., ground-penetrating radar) and remote sensing approaches (e.g., microwave technology) allow for the mapping of horizontal as well as vertical aquifers and soil water processes (Guo et al., 2014; Binley et al., 2015), and now make it easy to characterize the spatial variability of soil and bedrock topography (Vereecken et al., 2015; Guo et al., 2019).

Spatial structure and organization of land surface and subsurface characteristics present over a hierarchy of scales and control preferential flow processes within the soil pedon up to the catchment scale (Blöschl and Grayson, 2001; McDonnell et al., 2007; Korres et al., 2015). In general, three distinctive scales are recognized on the basis of three different conceptual and physical models for water flow in the vadose zone: pore scale, Darcian scale, and areal scale (Hendrickx and Flury, 2001). A common pore-scale preferential flow is saturated and unsaturated water flow through macropores and fractures. At the Darcian scale, unstable flow

68 occurs in water repellent soils as well as layered soil profiles, and preferential flow induced
69 by variability in soil hydraulic properties. At the areal scale, surface depressions and
70 discontinuous layers with lower or higher permeabilities can cause preferential flow. When
71 multiple spatial scales are involved, the features at a lower scale often form boundary
72 conditions for the processes acting at a higher scale (Bittelli et al., 2010). Currently, the
73 scales of spatial simulation models are usually too large to include the effects of lateral flow
74 on soil water (Fan et al., 2019). Especially in models of water movement in complex
75 landscapes, lateral flow due to differences either in anisotropic hydraulic conductivity or
76 topography should be taken into account (Buttle and McDonald, 2002; Maxwell and Kollet,
77 2008). Consequently, two- and three-dimensional modeling approaches will be more
78 appropriate for field situations where significant heterogeneity is displayed. However, few
79 models have been made to quantify the effects of soil heterogeneity and anisotropy combined
80 with scaling issues on hydrological fluxes (Ebel et al., 2007; Bittelli et al., 2010). Modelers
81 generally rely on plot-scale physical descriptions of water flow to describe the hillslope scale
82 water balance (Tromp-van Meerveld and Weiler, 2008). Comparisons of 2D and 3D
83 simulations of lateral flow convergence have shown that 3D simulation provide significantly
84 better results (Loague et al., 2006; Mirus et al., 2007; Fan et al., 2019).
85
86 Another challenge of hydrological models is the assessment of various uncertainties such as
87 expressions of soil and bedrock features, boundary conditions, as well as model structure that
88 is frequently ignored (Loos et al., 2007). Only a few models have included a permeable soil-
89 bedrock interface and even fewer have tested this assumption with experimental datasets
90 (Todd et al., 2000; Ebel et al., 2007; Camporese et al., 2019). As concluded by Tromp-van
91 Meerveld and Weiler (2008), the prevailing assumptions, that bedrock is impermeable and
92 soil depth is uniform, should always be questioned. While previous research has mostly
93 concentrated on uniform water flow with a single-porosity model, many experiments have
94 demonstrated the presence of nonequilibrium flow and transport conditions, which oftentimes
95 better described with dual-porosity models (Beven and Germann, 1982; Durner, 1994; Š
96 imůnek et al., 2006). Lateral flow occurring at the interface between soil and bedrock and/or
97 at the soil and hydrologically-impeding layers such as fragipans, has been recognized as an
98 important contributor to hillslope flow paths (e.g., Freer et al., 1997; Haga et al., 2005; Fan et
99 al., 2019). Laterally oriented macropore flow may dominate in areas where the macropores
100 are created by plant roots and burrowing animals (Newman et al., 1998; Gao et al., 2018).

These macropores may even enlarge by soil erosion, develop connectivity over several meters, and then potentially become soil pipes. Furthermore, the lateral subsurface flow on hillslopes was often triggered by a perched water table, which delivered water from hillslopes to valley floors (Maxwell and Kollet, 2008; Salve et al., 2012). In terms of this bedrock-influenced process, the fill and spill mechanism have been well used to explain threshold-driven hillslope responses (Tromp-van Meerveld and McDonnell, 2006; James et al., 2010; Camporese et al. (2019).

The last several decades have seen the model developments that consider non-equilibrium flow and transport, as well as the uncertainty issues (e.g., Buczko and Gerke, 2006; Heppner et al., 2007; Mirus et al., 2009). Using a number of virtual experiments with a 3D physics-based model, Hopp and McDonnell (2009) systematically investigated the interactions between some of the dominant controls on subsurface storm flow generation. However, their model still lacked predictions of subsurface preferential flow that would have been validated with actual measurements. While several studies have been conducted to compare various codes and approaches describing uniform Darcian flow in the vadose zone (e.g., Scanlon et al., 2002), similar comparisons simulating preferential and non-equilibrium flow are lacking (Larsson and Jarvis, 1999). An argument is that processes perceived to have an effect in the real system should also be represented in the model (Fatichi et al., 2016; Beven, 2001).

To clarify the extent and processes of preferential flow, we studied the dynamics of preferential flow in the forested Shale Hills watershed, where high temporal and spatial resolution monitoring of soil moisture is available. Previous studies at this critical zone observation site (Lin and Zhou, 2008) showed that the various landscape elements (i.e., hilltop, mid-slope, and hollows) differ greatly in soil texture and structure, and the subsurface preferential flow was occurred frequently (Zhao et al., 2012). We postulate that incorporating different soil types and their detailed spatial distributions into a physically-based model will enhance our understanding of water flow mechanisms and predictability of subsurface preferential flow. At the Panola Mountain Research Watershed, several physics-based modeling studies have taken into account the detailed representation of hydrologic and hydrostratigraphic variables (Hopp and McDonnell, 2009; James et al., 2010; Camporese et al., 2019).

We used multi-year datasets of three-dimensional soil moisture fields for our model test and evaluation. We employed the HYDRUS codes (Šimůnek et al., 2006), which include a hierarchical system of various approaches simulating preferential or non-equilibrium flow and transport in the vadose zone, starting from relatively simplistic approaches to the increasing complexity. HYDRUS is well tested and widely used in diverse applications (Scanlon et al., 2002; Kohne et al., 2004; Saito et al., 2006; Twarakavi et al., 2008; Šimůnek et al., 2016), where the remaining questions are regarding whether this small-scale physics-based model, fed with accurate data and representative scale, can properly simulate the behavior of complex hydrological systems (e.g., subsurface preferential flow) at the relatively large scale (Vereecken et al., 2015; Fatichi et al., 2016). Another similar question is how much complexity is really needed in hydrological models (Tromp-van Meerveld and Weiler, 2008)? Our objectives are: (1) to evaluate the ability of the dual-porosity and anisotropic models to describe preferential flow, (2) to elucidate how soil-bedrock geological conditions route subsurface preferential flow from top-ridge to the first-order stream, and (3) to assess the capabilities of multi-dimensional modeling in identifying the critical processes and parameters governing preferential flow. The elements are well tested individually, but not previously applied in such an integrated manner for water resources or environmental modeling applications.

# Materials and Methods

## Governing Flow Equation

In this study, we used the HYDRUS codes (HYDRUS-1D, HYDRUS-2D, and HYDRUS-3D) as a framework of various water movement simulations (Šimůnek et al., 2006). Here we briefly describe the main features of the model and those especially relevant parts for this study.

### Uniform Flow Model

The HYDRUS-3D solves the Richards' equation for water flow in saturated/unsaturated domains. The governing flow equation is a modified form of Richard's equation given as:

$$\frac{\partial \theta}{\partial t} = \frac{\partial}{\partial x_i}\left(K(K_{ij}^{A}\frac{\partial h}{\partial x_j} + K_{iz}^{A})\right) - S \qquad [1]$$

where $\theta$ is the volumetric water content ($L^3 L^{-3}$), $h$ is the pressure head (L), $S$ is a sink term ($T^{-1}$), $x_i$ (i = 1, 2, 3) are the spatial coordinates (L), $t$ is time (T), and $K_{ij}^A$ and $K_{iz}^A$ are components of a dimensionless anisotropy tensor $K^A$, and $K$ is the unsaturated hydraulic conductivity ($L\ T^{-1}$), respectively. We used the conventional van Genuchten-Mualem model (van Genuchten, 1980) for the hydraulic functions as follows:

$$S_e = \frac{\theta - \theta_r}{\theta_s - \theta_r} = \frac{1}{(1+|\alpha h|^n)^m} \quad [2a]$$

$$K = K_s S_e^l [1-(1-S_e^{1/m})^m]^2 \quad [2b]$$

where $S_e$ is the effective saturation, $\theta_s$ and $\theta_r$ are the saturated and residual water contents ($L^3\ L^{-3}$), respectively; the symbols $\alpha$ ($L^{-1}$), $n$, and $m$ = 1-1/$n$ are empirical shape parameters; $K_s$ is the saturated hydraulic conductivity ($L\ T^{-1}$), and $l$ is a pore connectivity parameter which normally is set to 0.5.

**Dual-Porosity Model**

In comparison with uniform flow (Eq. 1), dual-porosity models assume that water flow is partitioned into a macropore or fracture domain (the inter-aggregate pore domain) and a matrix domain (the intra-aggregate pore domain) where the water does not move at all (Šimůnek et al., 2003). This conceptualization leads to a two-region type flow models that partition the liquid phase into mobile (flowing, inter-aggregate), $\theta_{mo}$, and immobile (stagnant, intra-aggregate), $\theta_{im}$, regions [$L^3\ L^{-3}$]: $\theta=\theta_{mo}+\theta_{im}$. The dual-porosity formulation for water flow can be represented as (Gardenas et al., 2006):

$$\frac{\partial \theta_{mo}}{\partial t} = \frac{\partial}{\partial x_i}\left(K_{ij}\frac{\partial h}{\partial x_j} + K_{iz}\right) - S_{mo} - \Gamma_w \quad [3a]$$

$$\frac{\partial \theta_{im}}{\partial t} = -S_{im} + \Gamma_w \quad [3b]$$

where $S_{mo}$ and $S_{im}$ are sink terms for the mobile and immobile regions, respectively [$T^{-1}$], and $\Gamma_w$ is the water transfer rate between the inter- and intra-aggregate pore domains [$T^{-1}$]. The water mass transfer rate in [3b] is assumed to be proportional to the difference of the pressure head between the macropore and matrix regions (Gerke and van Genuchten, 1993b):

$$\Gamma_w = \alpha_w (h_f - h_m) \quad [3c]$$

where $a_w$ is a first-order mass transfer coefficient ($L^{-1}T^{-1}$):

$$\alpha_w = \frac{\beta}{d^2} K_a(h)\gamma_w \quad [3d]$$

where $d$ is an effective diffusion path-length (i.e., half the aggregate width) (L), $\beta$ is a shape factor that depends on the geometry of the soil aggregates (-), $\gamma_w$ is a scaling factor (-), and $K_a$ is the effective hydraulic conductivity of the fracture–matrix interface (L $T^{-1}$) determined as a simple arithmetic average involving both $h_f$ and $h_m$ as:

$$K_a(h) = 0.5[K_a(h_f) - K_a(h_m)] \quad [3e]$$

## Model Comparison

Empirically, the simulations of hydrological fluxes were affected by various uncertainties resulted from the soil hydraulic parameterization, from boundary conditions applied, and from the model structure (Loos et al., 2007). To evaluate model performance, we compared various model scenarios. First, model scales were differed into 1D, 2D, and 3D simulations through the HYDRUS hierarchical model approach; second, soil hydraulic parameters were represented either as uniform or as a dual-porosity flow; and third, the lower boundary conditions were set as fractured shale bedrock either a highly-weathered part (i.e., free drainage) or less-weathered, impermeable bedrock (i.e., no flux) (Tromp-van Meerveld et al., 2007).

### Experimental Site and Measurements

The model simulations presented here were based on field monitoring carried out at a 7.9-ha forested Shale Hills catchment, situated in central Pennsylvania, USA (Fig. 1), during a four-year period from 2007 to 2010. The Shale Hills catchment has a typical humid continental climate, with a minimum mean monthly temperature of –3°C in January, a maximum mean monthly temperature of 22°C in July, and the annual precipitation of about 980 mm (National Weather Service, State College, PA). The catchment is V-shaped overall, drained by a first-order stream in the valley and having moderately steep slopes of up to 25–48% on both sides of the stream. Elevation ranges from 256 m at the outlet of the catchment to 310 m at the highest ridge. The catchment is underlain by about 300-m thick, steeply bedded, highly fractured Rose Hill Shale, and covered by maple-oak-hickory vegetation.

The soils were formed from shale colluvium or residuum, with many channery shale fragments throughout most of the soil profiles that are silt loams and silty clay loams in texture (Table 1). Three soil series, according to the USDA classification, were identified in our investigated area (Table 1): (1) the Weikert series is a shallow, well-drained soil on the

steep planar hillslopes and summit regions, with depths to fractured shale bedrock less than 0.5 m; (2) the Rushtown series is a very deep, excessively drained soil at the center of concave hillslopes, with > 1 m depths to bedrock; and (3) the Ernest series is a very deep, poorly to moderately well-drained soil in the valley floor and around a first-order stream. Figure 1 shows the spatial distribution of the soil series along with a vertical transect.

For the field monitoring, sensors were installed at four sites (Figure 1, Table 1), which characterized by the following soil series: Weikert series on a hilltop (Site 74), Rushtown and Berks series at a mid-slope (Site 53), Rushtown series at the downslope of a swale (Site 51), and Blairton series close to the first-order stream that is at the outlet of a swale (Site 15). An array of sensors was installed at each site to measure soil water content, soil matrix potential, and soil temperature by soil horizons. For the preferential flow analysis, this paper mainly focused on the soil moisture data obtained with the ECH2O probes (Decagon Devices, Inc., Pullman, WA). A CR-10X datalogger (Campbell Scientific Inc., Logan, UT) was programmed to read data from the probes at 10-minute intervals with an accuracy of ±3% and a measurement resolution of 0.1%. Based on such high time-resolution measurements, we can evaluate whether preferential flow occurred by decoding the hydrograph of soil water content.

The subsurface preferential flow was assumed to have occurred when a subsurface soil horizon responded to a rainfall input earlier than a soil horizon above it (Lin and Zhou, 2008). Intuitively, when a soil moisture sensor buried in a subsoil responded to a storm event earlier than other sensors above it, the water had bypassed the overlying horizon(s) (i.e., vertical preferential flow) or had infiltrated into the deeper subsoil from the upslope or side-slope areas (i.e., lateral preferential flow). We wish to make quite clear that using the wording "subsurface preferential flow" implies structures that permit the types of macropore flow, unstable flow, funnel flow, etc. We recognized that there is no formulation of criteria for determining the preferential flow occurrence (Hendrickx and Flury, 2001; Nimmo, 2012). Our method might underestimate the occurrence of subsurface preferential flow since preferential flow does not necessarily require all the phenomena accounted for by our analysis.

To determine soil hydraulic properties (Table 2), representative soil horizons were sampled from each soil pit. Saturated hydraulic conductivities ($K_s$) were determined with the falling

head method using large, 30-cm diameter, undisturbed cores taken near the study hillslope (Lin et al., 2006). The water retention characteristics were determined by the pressure plate method, and parameters were fitted using RETC (van Genuchten et al., 1991). The soil texture, bulk density and total C-content were determined using disturbed soils (Zhao et al., 2010). The precipitation and weather variables required to estimate potential evapotranspiration were recorded by an *in-situ* automatic micrometeorological station. Root density, LAI and coverage of tree were also recorded monthly in this catchment.

**Model Domain, Initial and Boundary Conditions**

We designed the 3D simulated domain of 85 m length, 3 to 8 m width, and 1 to 4 m depth with a slope from 7% to 38% (Fig. 1 and Table 1). Based on soil horizon and soil sampling, the soil profiles were divided into 18 materials characterized by depth-related soil hydraulic properties, with four layers for the hilltop and four soil layers for the mid-slope, five layers for the down-slope (swale) and five layers for the outlet parts, respectively. Based on this, 2D simulation domain was considered as transect without width, and 1D simulation was the vertical soil profile with the heterogeneous soil layers at each of the four locations. The 3D model domain was implemented by importing the Shale Hills hillslope DEM (digital elevation model; x, y, z-coordinates of the surface and bedrock topography). Based on this geometric information, we generated a finite element mesh containing 46,200 nodes, and resulted in 80,959 3D elements in the form of triangular prisms. The transition into the deeper bedrock was represented by an inclined planar base surface (Fig. 1). The discretization of the model area is done by a triangular grid with the intersections of the adjoined triangles referred to as nodes. The grid was spaced <1 cm in the soil domain to ensure numerical stability with the grid being denser in the top soil and at the boundaries between layers.

Model initial conditions were set by linear interpolation of soil moisture at different depths measured at the beginning of the simulation date. The measured daily rainfall and calculated potential evapotranspiration (ET) were used as a time-variable atmospheric upper boundary condition of the model domain. Precipitation and potential ET were additionally corrected for the interception. Potential ET was estimated using the Hargreaves equation (Šimůnek et al., 2006). The upslope boundary and the two-edges of the domain along the slope were treated as no flux boundaries. A seepage face boundary condition was assigned to the entire width of the lower part of the domain, allowing water to leave the domain under zero potential. A free

drainage lower boundary condition was specified for the bottom of the model domain, assuming a unit total vertical hydraulic gradient. The minimum allowed pressure head was assumed as 1500 kPa at the upper boundary condition. Root water uptake was based on the model of Feddes et al. (1978). In general, the maximum rooting depth was designed to be 100 cm, with the greatest root density in the upper 50-cm soil depth.

**Implementation of Hydrological Simulation**

We first calibrated the HYDRUS-2D model using the two months data from July and August in 2007. For that calibration step, the measured soil hydraulic parameters were used as initial values for the simulations. We then did the inverse model to optimize the hydraulic parameters. The van Genuchten-Mualem parameters $\alpha$, $n$ and $K_s$ were adjusted during the calibration process based on our field measurements (Table 2). The calibrated parameters $\alpha$, $n$ and $K_s$ were then used as default values in the following calibration for the dual-porosity model (DP), where only $a_w$ was fitted while others (i.e., $\theta_s$ and $\theta_r$) were modified based on the values derived from the single-porosity model. The residual water content is equal to zero for the mobile region (i.e., residual water only present in the immobile region; Clothier et al., 1995). The calibrated parameters showed much better simulations than the measured one, that is, the peak trends and range of measured soil water were simulated reasonably (Fig. 2). Therefore, we used the calibrated parameters for the subsequent HYDRUS scenario simulations.

Our three-dimensional modeling approach is essentially corresponding to the three types of preferential flow occurred in three scales. In the 1D simulation (HYDRUS-1D) at the pedon scale, depth-related soil hydraulic parameters in the one-dimensional direction were used to represent unstable water flow due to the heterogeneous soil layers (e.g., macropore flow). In the 2D simulation (HYDRUS-2D) at the hillslope scale, we further considered that the hillslope elements from different sloped positions were connected, and allowed subsurface lateral flow to be considered (e.g., funnel flow due to impeding layer). The 3D simulation (HYDRUS-3D) at the catchment scale allowed us to consider lateral flow also from a sub-catchment (Hopp and McDonnell, 2009).

Based on data availability, we designed the simulation time for three temporal scales to cross-examine multi-dimensional modeling for various scenarios. The first time-scale investigated was minute-based representing the rapid response of water redistribution after rainfall, used

to evaluate the occurrence of preferential flow. The second time scale was daily-based representing the water dynamics associated with cycles of wetting and drying within a hydrological year, used basically to calibrate and validate the multi-dimensional modeling. The third time scale was yearly-based representing the water cycles over multiple years, used to check the power of model predictions for long-term time periods.

### Performance Assessment

In addition to graphical displays of simulated and measured results, statistical measures (root mean square error, *RMSE,* and the Nash–Sutcliffe efficiency, *NSE*) were used to evaluate the performance of the models (e.g., Ebel et al., 2007; Bittelli et al., 2010), as follows:

$$RMSE = \sqrt{\frac{1}{N}\sum_{i=1}^{N}(P_i - O_i)^2} \quad [4a]$$

$$NSE = 1 - \frac{\sum_{i=1}^{N}(P_i - O_i)^2}{\sum_{i=1}^{N}(O_i - \bar{O})^2} \quad [4b]$$

where $N$ is the number of observations, $P_i$ and $O_i$ are the simulated and measured values, respectively, and $\bar{O}$ is the mean of the observed values, respectively. The *RMSE* is inversely proportional to model efficiency with smaller *RMSE* values indicating higher model efficiency. The *NSE* efficiency statistic ranges between -∞ and 1, with 1 indicating a perfect match between observed and modeled values and less than zero indicating that the predicated value results in more error than using the average value of the observations.

# Results

### Evidence of Subsurface Preferential Flow

The soil moisture dynamics along the hillslope during a rainfall event are illustrated for a wetter period (Fig. 3) and a drier period (Fig. 4). In the wetter period, there are no indications of preferential flow in the Weikert soil at site 74 near the hilltop (Fig. 3a). This observation is consistent with the findings of Lin and Zhou (2008) who stated that during the wetter conditions the fractured shale of the R horizon did not respond earlier to storm events than any overlying soil horizons. However, in the drier period, this R horizon showed a clear response to the storm events, while other overlying soil horizons did not show any obvious response (Fig. 4a). This observation suggests that the storm water had somehow bypassed the overlying soil and infiltrated into the shale fractured rock and resulted in the preferential flow.

When there are rapid changes in soil water content within subsurface layers following a rain event and the upper layers reflect a delayed response in soil water content, the most probable explanation is that preferential flow has occurred.

In contrast, the overall subsurface preferential flow in the Berks soil at site 53 was infrequent during either drier or wetter periods. During the drier period, the deep C horizon at the 1.23-m soil depth displayed no indications of preferential flow and the C and B interface always responded considerably later to rainfall than the overlying Oe to Bw horizons (Fig. 3c). During the wetter period, there was more rapid water flow from the top to bottom of the soil profile that suggested a flush of water had easily reached the C horizon during the peak of the rain event (Fig. 4c). However, the deeper Rushtown soil at the middle of a swale at site 51 where preferential flow was frequent (Fig. 3b), displayed nearly an opposite trend as compared with site 53. During the drier period, a strong preferential flow was apparent at 0.18- and 0.25-m depths in the B horizon, where a rapid 2.0% increase in soil moisture that occurred 60 minutes after the start of the rain, while the horizons above and below the B horizon did not display a similar increase (Fig. 4b). This phenomenon suggests that some kinds of rapid lateral preferential flow had probably provided a flow path for the rainwater to this B horizon.

The Ernest soil at site 15 near the first-order stream was saturated for the entire wetter period except for the upper 13-cm topsoil layer, and therefore could not indicate any preferential flow through changes in its soil moisture content (Fig. 3d). The soil moisture contents generally displayed the usual wetting during rainfall infiltration until the layer reached saturation. During the dry period, however, preferential flow in some layers of this profile was observed (Fig. 4d). While A horizon at site 15 displayed very little change, the 2C to 4C horizons at the valley floor displayed a significant amount of increase in moisture contents, attributed to stormflow accumulated from the adjacent hillslope.

**Model Scale Associated with Preferential Flow Analysis**

Table 1 showed that soil horizons varied from loamy sand to sandy loam textures with indications of depth-dependent changes of the pedogenetic stratification. The changes in the soil textural profile influence the total porosity and the pore size distribution, as indicated by the depth-related hydraulic parameters (Table 2). For instance, the Weikert soil had a lower saturated water content ($\theta_s$) and a shallow R horizon while Rushtown had a large $\theta_s$ and a

deep soil profile. Those properties were parameterized and used in the numerical model following. Soil moisture was simulated using a multi-dimensional modeling approach for three temporal scales (Figs. 5-7). Regardless of the model approaches, the model performed well in simulating the general trend of field moisture observations. To compare different model approaches, the hydraulic properties and boundary conditions for each approach were parameterized as consistently as possible with independent measurements. We found that the most complex model provided the best predictions of the measured dynamics at each monitoring site. For instance, in the drier period (August 19-24), the subsurface preferential flow was described by 2D or 3D modeling approaches, but not by 1D simulation (Fig. 5). Especially, 3D modeling simulated the timing of the preferential flow occurrences accurately. We noticed that 3D simulations at site 74 showed a lag time of about 6 h behind the measured data, which is due to the delayed rainfall input from canopy and/or litter interception. For 1-yr hydrological simulations (Fig. 6), the one-dimensional model underestimated the soil moisture because it did not consider the lateral flow contributions. In contrast, the 2D simulation, which considered the sloped-topographic effects, could reflect the occurrence of preferential flow. However, the 2D simulations did not perform as well as the 3D simulations when comparing predicted daily values and field measurements. The 3D simulations provided the best predictions of the measured values although there are still some differences that are largely attributed to the spatial variability inherent in hydrological processes.

Although model calibration represented one level of testing to reproduce field data, the model may not be applied to field conditions that are significantly different than the conditions under which calibration were conducted. For these reasons, it is important to test the predictive capabilities of a model beyond the calibration period. Figure 7 showed the 2D simulation for the 4-yr period, which basically showed the a very similar predictive power with the 1-yr simulation, indicating the current model is capable of simulating the hydrological processes for the long-term time period.

The 3D model enabled predictions to be obtained for soil water content distributions at each location and time, with the consideration of the full 3D issue (e.g., the ability to consider convergent lateral inflows). An example of a three-dimensional representation of pressure head on August 20, 2007 is shown in Figure 8, indicating a higher water potential in the downslope positions or in the topsoil depths. Furthermore, we selected a transect of simulation on the same date to show representative subsurface lateral flow after rainfall

events (Fig. 9). In this example, subsurface preferential flow in the shallow Weikert soil occurred in the R horizon while in the deep soil such as the Rushtown, it occurred in the Bw and C horizons. The increases in soil moisture indicate that the water infiltrated into the bedrock fractures below the shallow Weikert soil and moved laterally to the deep horizons of the downslope Rushtown soil. To our best knowledge, this is one of few attempts to simulate the preferential flow pathways at the sloped catchment successfully.

**Parameterization of Soil Properties**

We examined the significance of subsurface lateral flow comparing the governing equations for both equilibrium water flow in a uniform porosity (i.e., without macropore flow) and nonequilibrium flow in a dual-porosity system (i.e., with macropore flow). The uniform porosity and dual-porosity approaches both reflected the soil moisture dynamics throughout a hydrological year (Fig. 10). However, the dual-porosity model provided much improved simulations, and indicated that considering the fracture-matrix structure in the dual-porosity model provided better predications. The prominence of subsurface preferential flow in this catchment is also supported by the anisotropic $K_s$ reported in a previous study (Lin et al., 2006). There were large differences in the lateral and vertical $K_s$, e.g., the $K_h$ (i.e., the horizontal $K_s$) is higher than the $K_v$ (i.e., the vertical $K_s$) in the B layer and in the vicinity of the bedrock fractures (Table 2). This difference is clearly ascribed to the presence of a platy structure due to the geological formation of a longer horizontal axis leading to a higher continuity of horizontal direction along the aggregates/fractures. To illustrate the consequences of anisotropic hydraulic properties on subsurface preferential flow, the model results using anisotropic $K_s$ are compared with the model output from isotropic $K_s$. For some unmeasured horizontal hydraulic conductivities that are attributed to the fractured bedrock, we used a value of the horizontal $K_s$ that is 10 times the vertical $K_s$. Figure 11 shows that the simulations improved once the anisotropic was considered, and indicates that anisotropy significantly contributed to the rapid subsurface flow.

**Boundary Conditions**

To examine the effect of a permeable boundary condition (BC) at the weathered bedrock boundary, another hydrologic-response simulation of impermeable BC was explored. An impermeable boundary was designed as a no flux boundary condition, while a permeable BC was mimicked using a free drainage condition which assumed the groundwater level is far away from the bottom of the model domain. At site 51, a permeable BC provides better

460 predictions than when an impermeable BC is taken into account (Fig. 12b and Table 3),
461 indicating that actual field conditions should be characterized by a fracture-structured shale
462 geology. However, at site 74, an impermeable BC provided better predictions than when a
463 permeable BC was assumed and implied that site 74 was characterized by a soil-bedrock
464 interface (Fig. 12a).
465
466 These results illustrate that the parameterization of fractured shale geology is important to
467 accurately simulate the occurrence of preferential flow. In general, the bedrock is typically
468 simulated by setting an extremely low value of $K_s$ and results in the formation of perched
469 water tables. However, bedrock layers in our study area are often fractured with values of
470 hydraulic conductivity changing in the horizontal direction that adds to the variability of
471 vertical water fluxes. These differences may help explain some discrepancies between the
472 simulated and the measured water contents, particularly during the wet spring periods at the
473 site 15 (Fig. 6d), when there are arising perched water depths. In our case, the perched water
474 depths existed because of the presence of a shallow fractured layer. Figure 13a shows that the
475 model performed well in simulating the water table dynamics well at site 15. However,
476 groundwater recharge into the soil was not fully considered in our model, and therefore
477 resulting in weak predictions of water dynamics for site 15. Lin et al. (2006) described a
478 discontinuity in the fragipan and noted that a significant error in perched water depths can be
479 caused by a very small error in simulated soil water contents, and vice versa. Furthermore,
480 Figure 13b shows the measured discharge at the outlet of the catchment (Fig. 1) and
481 simulated discharge in the sub-catchment accounted by this study (i.e., our 3D domain).
482 Although the values can not be directly compared since the model did not included the spatial
483 scale of the whole catchment, the similar trends and dynamics displayed in responding to
484 rainfall should have indicated that our simulated drainage was sensitive.
485
486 The model performance is also indicated by the *NSE* and *RMSE* parameters (Tables 3). The
487 *RMSE* values are all smaller than 0.1, with the 3D simulations having the lowest bias and the
488 1D simulations having the highest bias. Similarly, the *NSE* values range from -3.8 to 0.74,
489 with the 3D simulation having the most favorable expectations. The results in the right part of
490 Table 3 seem to agree with the trends previously observed in the figure. We noticed that
491 some *NSE* values are below zero that may illustrate the effect of a few very poorly simulated
492 values in biasing the *NSE* (Ebel et al., 2007). Examination of Table 3 also confirms that the
493 single-porosity model does not perform as well as the dual-porosity model, and considering

anisotropic $K_s$ improves the simulations. While no flux BC resulted in more accurate prediction results for site 74 characterized by impermeable bottom bedrock geology, free drainage BC resulted in improved model results for site 51 characterized by permeable fractured geology.

For the calculated hydrological year 2007, the simulated water balance in our sub-catchment indicated that 38% of the precipitation was drained (of which 6% was seepage flux and 32% was streamflow), 35% was evaporated, 19% was transpirated, and 8% was stored in the soil. Overland flow was a small portion and only occurred after higher rainfall intensity events (Fig. 14). Actual evapotranspiration was relatively large for the maple-oak-hickory vegetation compared to the amount of subsurface drainage. However, considering the relatively small rainfall volumes, the drainage is high.

# Discussions

### Multi-dimensional Modeling Approach in Identifying Subsurface Preferential Flow

Direct evidence of preferential flow was obtained by comparing the dynamics in the measured soil moisture contents and was further validated by the numerical simulations. Variations in soil moisture are thought to be governed by internal properties and external influences (Comporese et al., 2019). During 1D simulation, the external influences are generally identified as input and output fluxes in the vertical dimension. During 2D simulation, output fluxes from adjacent spatial units are commonly input fluxes to the neighboring spatial units, and have been referred to as a catenary linkage along the slopes (Zepp et al., 2005). Therefore, one-dimensional hydrological modeling has one general disadvantage in that lateral water fluxes may not be taken into account.

The advantages of considering lateral water movement are displayed in our 2D and 3D simulation results, which reflect the occurrence of subsurface preferential flow in the shallow Weikert soil and deep Rushtown soil. However, the 2D simulations did not perform as well as the 3D simulations in predicting the moisture dynamics and that were influenced by the occurrence of preferential flow. During the 3D simulations, the lateral flow from the surrounding units strongly contributed to the moisture dynamics, especially in the concave hillslope position (site 51). This finding is consistent with the previous analysis that a high frequency of lateral/inter-connected flow occurred in this sloped forest (Grahamm and Lin,

2011). However, simulation of three-dimensional water transport in structured soils has previously been restricted primarily due to the numerical complexity (Loague et al., 2006; Mirus et al., 2007). Our study indicates that it is necessary to perform 3D simulations to adequately describe the water components and pathways in the hillslope subsurface hydrology, especially in the presence of preferential flow.

It was determined that hyper-resolution monitoring data of soil moisture may be used to address the occurrence of subsurface preferential flow at the point scale. Combined with a model survey, potential spatial flow patterns may be identified, flow mechanisms may be confirmed, and flow pathways may be documented at the hillslope scale (Sidle et al., 2001; Salve et al., 2012; Fan et al., 2019). Similar to Comporese et al. (2019), our results also show an initial soil moisture threshold must be attained to initiate subsurface preferential flow. Soil moisture in the dry season is about 10% and following rainfall events, subsurface preferential flow occurred in the upslope position (site 74), the down slope position (site 51), and in the valley floor (site 15). In contrast, during the wetter period (soil moisture is about 15%), site 74 did not show the occurrence of preferential flow and only the down slope position at site 51 indicated a weak occurrence. Therefore, this confirms that shifting control of hillslope soil-terrain attributes on the soil water content distribution under different states. During the drier period at site 74, water bypassing the upper horizons and reaching the R horizon was probably related to the water repellency of the organic litter coverage or may have originated in the upslope or the sideslope (Lin et al., 2006).

**Characterizing Soil and Bedrock Properties in the Models**

There are numerous evidences showing flow processes in soils often can be better described using non-equilibrium two-domain models rather than classical single-domain models (e.g., Šimůnek et al., 2003; Kohne et al., 2004). Here we exploit a dual-porosity model by assuming that water in the soil particles or aggregates is immobile, but that the soil is allowed to dry out or rewet during drying and wetting processes. Our results confirm that, in comparison with a single-domain model, dual-porosity models do perform well in describing the processes involved within the local soil subsurface macropore network and are better representing the dynamics of soil moisture (McDonnell et al., 2007). Such models, however, cannot predict preferential flow since there are no mechanisms to account for lateral non-equilibrium flow. In the Shale Hills Catchment, shallow tree rooting systems that branch

horizontally-oriented shale bedrock alter the flow direction and the pore continuity, and favor the development of lateral preferential flow systems in the soil (Grahamm and Lin, 2011).

Our inability to accurately estimate the geometry prevented detailed assessments of the weathered bedrock water table response and discharge at the lower outlet weir (Fig. 13). The more sophisticated geological characterization will be needed to improve model predictions (Rakovec et al., 2016). One of the critical questions might be how much model complexity is needed to explain the data while realizing that the data may be insufficient to test a model structure adequately. Although the bedrock is typically assumed as an impermeable layer in numerical models, there is evidence indicating that bedrock sometimes is permeable (e.g., Comporese et al., 2019). Our results show that actual field conditions may be more accurately characterized by considering both a permeable fracture-structured shale bedrock (e.g., site 51) and an impermeable bedrock (e.g., site 74), and we further demonstrate that the parameterization of fractured shale geology is important to accurately simulate the occurrence of preferential flow. Our finding are also corroborated by Ebel et al., (2007), who indicated that representing layered geologic interfaces by an impermeable boundary condition leads to large prediction errors. Several other researchers have also documented the role of soil-bedrock interfaces as important hillslope flowpaths (e.g., Freer et al., 1997; Onda et al., 2001).

We also confirm during 2D simulations that if anisotropic $K$ existed, the direction of movement and quantity of soil water differed from the simulations that of assumed an isotropic $K$. In examining the measured soil moisture data, the direction of water movement is almost parallel to the lateral slope (Guo et al., 2019). This observation might help to explain why the simulations that consider the anisotropy of $K_s$ produce better prediction results than the simulation results that considered $K_s$ as being isotropic. The inference is that the anisotropic behavior of $K_s$ is more realistic in representing the macroporosity found in the structured soil. Some authors (e.g., Newman et al., 1998; Beckwith et al., 2003) have also mentioned that soils consisting of fine layers parallel to the surface, like stratified soils, exhibited a horizontal $K_s$ greater than its vertical $K_s$. It is expected that omitting the anisotropy in hydraulic parameters will negatively affect simulation results, especially in the fractured zone (Ebel et al., 2007; James et al., 2010). The anisotropy of $K_s$ across the whole catchment implied that there exists a dominant lateral flow pathway that delivers water from the hilltop to the valley floor.

**Pathway and Connectivity along the Hillslope**

Soil layering may have large impacts on the occurrence of subsurface preferential flow because significant changes in texture across the boundary of two adjacent layers could noticeably alter water distribution (Comporese et al., 2019). The changes in soil moisture over time indicated that subsurface preferential flow that occurred in the upslope may have delivered water to the middle slope and finally the water reached the valley floor due to the extensively fractured bedrock structure (Liu and Lin, 2015). Our modeling results provided evidence that water within the soil horizons may rapidly infiltrate at each site, and then form potential pathways within the entire sloped transect.

The first pathway was initiated when the rainfall infiltrated the shallow fractured shale bedrock at the upslope, where water move laterally, recharge the Bw and C horizons of the mid-slope and downslope, and finally recharge the Bt horizon and the C horizon of the valley floor. The modeling results indicated that the general flow patterns were different between the soil types and within the hillslope positions. While subsurface lateral macropore flow was dominant in the shallow Weikert soil in the planar uphill position, a combination of vertical macropore flow and lateral matrix flow was dominant in the deep Rushtown soil in the concave midslope position.

A second pathway had water moving through the fracture and directly recharging the deep C horizon at the downslope and valley floor sites. The simulation results indicated that preferential flow in the deep C horizon was initiated by water within the bedrock fracture and that water moved laterally under the slope gradient on the top of the underlying impeded layer. This constituted a hydrological pathway for rapid lateral flow above the groundwater zone. It is also likely that a perched water table developed in the shallow subsurface and resulted in the water flow towards the downslope position, as was indicated by a rapid rise of topsoil water after large precipitation events at site 15 (Fig. 13a). The presence of a perched water table indicated that the vertical percolation locally exceeded the $K_s$ at the perching layers and suggested that flow paths may not be vertical through the entire thickness of the unsaturated zone. Instead, water may have been diverted laterally to a fault zone or another high-permeability channel that served to channel flow downward to the water table.

We found that the anisotropy of $K_s$, coupled with the moderate slopes, the clay-enriched Bt horizons in the Rushstown and Ernest series, and the shallow soil–bedrock interface throughout much of the catchment hillslopes, contributed to significant subsurface lateral water movement. Even though individual macropores were rather short, the coupling of these flow paths with the bedrock fractures, living and decayed roots, and perched water tables produced networks of interconnected preferential flow pathways, all of which help explain the preferential flow observed in the catchment (Hopp and McDonnell, 2009; Guo et al., 2014; Gao et al. 2018). The connectivity of flowpaths is highly related not only to the soil-bedrock properties but also to the initial moisture content (Salve et al., 2012). Although preferential flow occurred at each site, only a few rainfall events indeed demonstrated the connectivity from the hilltop to the valley floor (Lin and Zhou, 2008). These observations suggested that during dry conditions, the flowpaths for the occurrence of subsurface preferential flow are only 'locally' connected and cannot deliver water through long distances to the valley floor. Soil moisture at certain hillslope locations may work as important "nodes" and the soil horizon may function as a "path" in the subsurface flow network. In certain conditions, such as high soil moisture contents and strong and/or long duration rainfall, the "nodes" may be activated and deliver water downslope through the "path" (Guo et al., 2014). Sidle et al. (2001) reported self-organization of preferential flow on forested hillslopes where individual short flow paths are linked via a series of 'nodes' that may be switched on and off and/or expand and shrink in response to local changes in soil moisture conditions. However, disconnected macropores may connect hydraulically during storms and result in an effective drainage of hillslopes (Tromp-van Meerveld and McDonnell, 2006; Lehmann et al., 2007). Further assessment of the propensity for preferential flow is necessary to determine how antecedent soil water content affects the flow processes as a function of precipitation amount and intensity.

For a conceptual understanding, even though the mechanisms that lead to the formation of preferential flow patterns are very different when evaluated at different spatial scales, the occurrence of preferential flow and the environmental consequences are often very similar. In Figure 15 we present a flow diagram for the evaluation of vadose zone conditions that will cause preferential flow at different positions as a result of a lateral flow trigger. Since precipitation is spatially uniform, it will result in uniform one-dimensional flow through the vadose zone unless a lateral flow trigger is present. We recognize that different lateral flow triggers may exist such as a precipitation rate that exceeds the infiltration rate, vertical

changes in unsaturated hydraulic conductivities where the lower layer has a lower conductivity, water repellency, and other mechanisms that cause unstable flow.

**Implications**

In this study, we compared different conceptual hydrological approaches for their ability to simulate the preferential flowpaths in soils. Based on the monitoring evidence of preferential flow and identification of geomorphogical conditions, coupled with the quantitative soil moisture dynamics using a multi-dimensional modeling approach, we confirmed our former assumption that subsurface lateral flow is the primary flow mechanism in this catchment (Lin et al., 2006). Two types of subsurface lateral flow were identified as dominating hydrological features which were highly controlled by multiscale behavior of the intrinsic soil and fracture system, in addition to initial wetness conditions as well as rainfall characteristics. The HYDRUS model results provide an excellent approximation that describes potential hydrologic flowpaths for a complex hillslope underlain by fractured bedrocks, with complex flow pathways and limited geomorphogical parameterization for the simulation. The simulations reported herein demonstrate that physically-based models, like HYDRUS, are capable of characterizing detailed spatio-temporal hydrologic responses, developing the concepts of the process-based multiscale model, and for representing preferential flowpaths by a Darcian dual-continuum approach. The field-based observations and hydrologic-response simulations from the Shale Hills catchment highlight the evidence in characterizing/simulating fractured bedrock flow within a complex small catchment and have important implications for understanding hydrologic response in these types of catchment basins.

In comparison with the former researches, our modeling application led to several improvements. The first but not last improvement in this study is the full 3D simulation parameterized by the detailed field observations, followed by validation via the experimental data, which provides greater feedback for the understanding of process-based concepts (Fan et al., 2019). In the past, a physical-based model like HYTDRUS may only be applied in the small scale or in the relatively simple geomorphogical conditions. The second improvement is the characterization of soil hydraulic properties that includes preferential flow via macropores and fractures, and a more accurate description of the subsurface as a multi-layer soil profile above the bedrock (Rakovec et al., 2016). Comparison of hydrologic-response simulations using lab measured soil-water retention curves versus inversely estimated

parameters based on measured soil moisture data analysis showed that in situ field-based data calibration can dramatically improve simulation. The third improvement is the explicit consideration of the anisotropy of hydraulic parameters. This is a challengeable area given the near impossibility of making the field measurements to assess how soil anisotropy and bedrock permeability might be necessary for evaluating preferential flow (McDonnell et al., 2007; James et al., 2010; Camporese et al., 2019). The fourth improvement is the variable representation of boundary conditions (Camporese et al., 2019). Uncertainty analyses demonstrated that modeling layered geologic interfaces with an impermeable BC leads to substantial inaccuracies, considering many forest hillslopes composed of relatively thin, permeable soil mantles overlaying less-permeable bedrock.

However, our model approach may not well reproduce bedrock-controlled threshold responses such as the fill and spill process, as observed by other hillslope scale studies (Tromp-van Meerveld and McDonnell, 2006; Hopp and McDonnell, 2009; James et al., 2010). Recently, Camporese et al. (2019) confirmed that Richards equation-based numerical model (CATHY) are able to generate such responses at the well-characterized Panola experimental hillslope in Georgia (USA). It is promise to further investigate either whether the widely-used and Richards equation-based numerical model HYDRUS is able to reproduce threshold mechanisms or to what extent the fill-and-spill process exists in a well-gauged Shale Hills catchment (Guo et al., 2019). Given the potentially broad applicability of the fill-and-spill model, it is valuable to define the scale of interest first and then investigate if and how fill and spill manifest at that scale so as to include those details in the model parameterization (Comporese et al., 2019). Based on the ground-penetrating radar survey, Guo et al. (2019) recently established a conceptual model of subsurface runoff generation to describe the roles of preferential flow in subsurface hydrology at the Shall Hills catchment. Interestingly and importantly, our model could potentially help not only in the further model development of Critical Zone hydrology but also in many practical purposes, such as moisture storage in the fractured rock that is important for supporting vegetation growth (Guo et al., 2019). For instance, Maxwell (2020) addressed that the lateral subsurface flow may have provided a downslope water source for plants during dry times, which could be fully accounted by the HYDRUS model or its extension since those physically-based itself have well incorporated the flexible root water uptake module, as well as the interactions within soil-landscape features across the sloped catchment. This is expected to be figured out in following-on work.

Earth System Models are essential tools for understanding the dominant hydrological processes, but they cannot explicitly resolve the first-order structures and functions that fundamentally organize water and energy across the landscapes (Fan et al., 2019). Process understanding, data collection and model development should be linked so that a more complete representation with each iteration was reasonably obtained (Grayson and Blöschl, 2000). Currently, the limited availability of the less-than-perfect observed data sets has restricted the field validation of preferential flow models. Without detailed field measurements, it is unlikely that our modeling approach would have identified fractured bedrock flow as an essential process. Provided such data are available, our results indicate that physically-based models, like HYDRUS, when properly parameterized, can simulate catchment-scale water flow.

## Conclusions

In this showcase application, we compared increasingly complex models with a consistent dataset and concluded that a multi-dimensional modeling approach helped to elucidate how dominate hydrological processes related to soil-landscape features in a small catchment. Soil moisture monitoring indicated the existence of a subsurface flow network, which was influenced by soil properties such as soil type, soil depth, permeability, and soil location that controlled locally occurring subsurface preferential flow. The model results verified that detailed characterization of soil and weathered bedrock thickness and hydraulic properties is critical for simulating pore-water pressure generation at sites like Shale Hills where convergent subsurface flow and fracture flow is important. When preferential flow was considered in 2D and 3D simulations, it improved the accuracy of model predictions. We confirmed that the dual-porosity model is better than the single-porosity model because it can better represent macropores in the soil, with consideration of anisotropic $K_s$ further improving the model accuracy. Models considering the presence of fractured bedrock performed better than when this was not considered and demonstrated that the actual field conditions were characterized by fractured or perched geology. This study summarily enhanced understanding of mechanisms, actual locations and potential flow pathways of subsurface preferential flow in a forested catchment via multi-dimensional process-based hydrological modeling.

## Acknowledgments

This research was supported in part by the U.S. National Science Foundation through the Shale Hills Critical Zone Observatory grant (EAR-0725019), Taishan Scholars Program (201812096) and the National Natural Science Foundation of China (41977009). Fei Li was supported by the Agricultural Science and Technology Innovation Program of CAAS (CAAS-ASTIP-2020-IGR-04). Data were provided by the NSF-supported Southern Sierra Critical Zone Observatory. The data set is available at http://criticalzone.org/shale-hills/data/datasets/. Assistance in field data collections from the Penn State Hydropedology Group, and suggestions of Markus Flury from Washington State University and Jeffrey J. McDonnell from University of Saskatchewan are gratefully acknowledged.

## References

Beckwith, C.W., A.J. Baird, and A.L. Heathwaite. 2003. Anisotropy and depth-related heterogeneity of hydraulic conductivity in a bog peat. II: Modelling the effects on groundwater flow. *Hydrological Processes*, 17, 103–113.

Beven, K., 2001. On explanatory depth and predictive power. *Hydrological Processes*, 15, 3069–3072.

Beven K., and P. Germann. 2013. Macropores and water flow in soils revisited. *Water Resources Research*, 49, doi:10.1002/wrcr.20156.

Beven K., and P. Germann. 1982. Macropores and water flow in soils. *Water Resources Research*, 18, 1311-1325.

Blöschl, G., and R.B. Grayson. 2001. Spatial Patterns in Catchment Hydrology: Observations and Modelling, 416 pp., Cambridge Univ. Press, New York.

Clark, M.P., Fan, Y., Lawrence, D.M., Adam, J.C., Bolster, D., Gochis, D.J., et al. 2015. Improving the representation of hydrologic processes in Earth System Models. *Water Resources Research*, 51, 5929–5956. https://doi.org/10.1002/2015WR017096.

Grayson, R., Blöschl, G., 2000. Spatial modelling of catchment dynamics. In: Grayson, R., Blöschl, G. (Eds.), Spatial Patterns in Catchment Hydrology: Observations and Modelling. Cambridge University Press.

Binley, A., Hubbard, S.S., Huisman, J.A., Revil, A., Robinson, D.A., Singha, K., & Slater, L.D. 2015. The emergence of hydrogeophysics for improved understanding of subsurface processes over multiple scales. *Water Resources Research*, 51, 3837–3866. https//doi.org/10.1002/2015WR017016.

Bittelli, M., F. Tomei, A. Pistorcchi, M. Flury, J. Boll, E.S. Brooks, and G. Antolini. 2010. Development and testing of a physically based, three-dimensional model of surface and subsurface hydrology. *Advance in Water Resources*, 33, 106–122.

Buttle, J.M., and D.J. McDonald. 2002. Coupled vertical and lateral preferential flow on a forested slope. *Water Resources Research*, 38:1060, doi:10.1029/2001WR000773.

Buczko, U., and H.H. Gerke, 2006. Modeling two-dimensional water flow and bromide transport in a heterogeneous lignitic mine soil. *Vadose Zone Journal*, 5, 14–26.

Camporese, M., Paniconi, C., Putti, M., & McDonnell, J.J. 2019. Fill and spill hillslope runoff representation with a Richards equation-based model. *Water Resources Research*, 55. https://doi.org/10.1029/2019WR025726.

Durner, W. 1994. Hydraulic conductivity estimation for soils with heterogeneous pore structure. *Water Resources Research*, 30, 211–233.

Ebel, B.A., K. Loague, J.E. Vanderkwaak, W.E. Dietrich, D.R. Montgomery, R. Torres, and S.P. Anderson. 2007. Near-surface hydrologic response for a steep, unchanneled catchment near Coos Bay, Oregon: 2. Physics-based simulations. *America Journal of Science*, 307, 709–748.

Fan, Y., Clark, M., Lawrence, D. M., Swenson, S., Band, L. E., Brantley, S. L., et al. 2019. Hillslope hydrology in global change research and Earth System Modeling. *Water Resources Research*, 55, 1737–1772. https//doi.org/10.1029/2018WR023903.

Feddes, R.A., P. Kabat, P.J.T. van Bakel, J.J.B. Bronswijk, and J. Halbertsma. 1988. Modelling soil water dynamics in the unsaturated zone-State of the art. *Journal of Hydrology*, 100, 69–111.

Feddes, R.A., P.J. Kowalik, and H. Zaradny. 1978. Simulation of field water use and crop yield, John Wiley and Sons, New York, NY.

Freer, J., McDonnell, J.J., Beven, K.J., Brammer, D., Burns, D., Hooper, R. P., and Kendall, C. 1997. Topographic controls on subsurface storm flow at the hillslope scale for two hydrologically distinct small catchments. *Hydrological Processes*, 11, 1347–1352.

Freeze, R.A. 1972. Role of subsurface flow in generating surface runoff 1. Base flow contributions to channel flow. *Water Resources Research*, 8, 609–624.

Gardenas, A.I., J. Šimůnek, N. Jarvis, and M.Th. Van Genuchten. 2006. Two-dimensional modelling of preferential water flow and pesticide transport from a tile-drain field. *Journal of Hydrology*, 329, 647–660.

826 Gao, M., Li, H.-Y., Liu, D., Tang, J., Chen, X., Chen, X., Blöschl, G., and L.R. Leung. 2018.
827 Identifying the dominant controls on macropore flow velocity in soils: A meta-analysis.
828 *Journal of Hydrology*, 567, 590–604.
829 Gerke, H.H., and M.T. van Genuchten. 1993a. A dual-porosity model for simulating the
830 preferential movement of water and solutes in structured porous media. *Water Resources*
831 *Research*, 29, 305–319.
832 Gerke, H.H., and M.T. van Genuchten. 1993b. Evaluation of a first order water transfer term
833 for variably saturated dual-porosity flow models. *Water Resources Research*, 29, 1225–
834 1238.
835 Graham, C., and H.S. Lin. 2011. Controls and frequency of preferential flow occurrence at
836 the Shale Hills Critical Zone Observatory: A 175 event analysis of soil moisture
837 response to precipitation. *Vadose Zone Journal*, 10, 816–831.
838 Gu, W.Z., J.F. Liu, H.S. Lin, J. Lin, H.W. Liu, A.-M. Liao, N. Wang, W.Z. Wang, T. Ma, N.
839 Yang, X.G. Li, P. Zhuo, and Z. Cai. 2018. Why hydrological maze: The
840 hydropedological trigger? Review of experiments at Chuzhou Hydrology Laboratory.
841 *Vadose Zone Journal*, 17, 170174. doi:10.2136/vzj2017.09.0174.
842 Guo, L., H.S. Lin, and J. Chen. 2014. Subsurface lateral flow network on a hillslope revealed
843 by time-lapse ground penetrating radar. *Water Resources Research*, 50, 9127–9147.
844 Guo, L., H. Lin, B. Fan, J. Nyquist, L. Toran, G. Mount. 2019. Preferential flow through
845 shallow fractured bedrock and a 3D fill-and-spill model of hillslope subsurface
846 hydrology. *Journal of Hydrology*, 576, 430–442.
847 Kohne, J.M., B. Mohanty, J. Šimůnek, and H.H. Gerke. 2004. Numerical evaluation of a
848 second-order water transfer term for variably saturated dual-permeability models. *Water*
849 *Resources Research*, 40:W07409, doi:10.1029/2004WR003285.
850 Korres, W., T.G. Reichenau, P. Fiener, C.N. Koyama, H.R. Bogena, T. Cornelissen, R. Baatz,
851 M. Herbst, B. Diekkrüger, H. Vereecken, and K. Schneider. 2015. Spatio-temporal soil
852 moisture patterns-A meta-analysis using plot to catchment scale. *Journal of Hydrology*,
853 520, 326–341.
854 Haga, H., Y. Matsumoto, J. Matsutani, M. Fujita, K. Nishida, and Y. Sakamoto. 2005. Flow
855 paths, rainfall properties, and antecedent soil moisture controlling lags to peak discharge
856 in a granitic unchanneled catchment. *Water Resources Research*, 41, W12410,
857 doi:10.1029/2005WR004236.

858 Hendrickx, J.M.H., and M. Flury. 2001. Uniform and preferential flow, mechanisms in the
859 vadose zone, Conceptual Models of Flow and Transport in the Fractured Vadose Zone,
860 National Research Council, National Academy Press, Washington, DC, pp. 149–187.
861 Heppner, C.S., K. Loague, and J.E. VanderKwaak. 2007. Long-term InHM simulations of
862 hydrologic response and sediment transport for the R-5 catchment. *Earth Surface*
863 *Process and Landform*, 32(9), 1273–1292.
864 Hopp, L., and J.J. McDonnell. 2009. Connectivity at the hillslope scale: Identifying
865 interactions between storm size bedrock permeability, slope angle and soil depth.
866 *Journal of Hydrology*, 376, 378–391.
867 Larsson, M.H., and N.J. Jarvis, 1999. Evaluation of a dual-porosity model to predict field-
868 scale solute transport in a macroporous soil. *Journal of Hydrology*, 215, 153–171.
869 Lehmann, P., C. Hinz, G. McGrath, H.J. Tromp-van Meerveld, and J.J. McDonnell. 2007.
870 Rainfall threshold for hillslope outflow: an emergent property of flow pathway
871 connectivity. *Hydrology and Earth System Sciences*, 11, 1047–1063.
872 Lin, H. 2006. Temporal Stability of Soil Moisture Spatial Pattern and Subsurface Preferential
873 Flow Pathways in the Shale Hills Catchment. *Vadose Zone Journal*, 5, 317–340.
874 Lin, H. and X. Zhou. 2008. Evidence of subsurface preferential flow using soil hydrologic
875 monitoring in the Shale Hills catchment. *European Journal of Soil Science*, 59, 34–49.
876 Liu, H. and H.S. Lin. 2015. Frequency and control of subsurface preferential flow: from
877 pedon to catchment scales. *Soil Science Society of America Journal*, 79, 362–377.
878 Loague, K., C.S. Heppner, B.B. Mirus, B.A. Ebel, Q. Ran, A.E. Carr, S.H. BeVille, and J.E.
879 VanderKwaak. 2006. Physics-based hydrologic-response simulation: Foundation for
880 hydroecology and hydrogeomorphology. *Hydrological Processes*, 20(5), 1231–1237.
881 Loos, C., S. Gayler, and S. Priesack. 2007. Assessment of water balance simulations for large
882 scale weighing lysimeters. *Journal of Hydrology*, 335, 259–270.
883 Maxwell, R.M. 2020. Water colour and climate. *Nature Climate Change*, 102–103.
884 Maxwell, R.M., and S.J., Kollet. 2008. Interdependence of groundwater dynamics and land-
885 energy feedbacks under climate change. *Nature Geoscience*, 1, 665–669.
886 McCord, J.T., D.B. Stephens, and J.L. Wilson. 1991. Hysteresis and state-dependent
887 anisotropy in modeling unsaturated hill slope hydrologic processes. *Water Resources*
888 *Research*, 27, 1501–1518.
889 McDonnell, J.J., Sivapalan, M., Vaché, K., Dunn, S.M., Grant, G., Haggerty, R., Hinz, C.,
890 Hooper, R., Kirchner, J., Roderick, M.L., Selker, J., Weiler, M. 2007. Moving beyond

heterogeneity and process complexity: a new vision for watershed hydrology. *Water Resources Research*, 43, W07301, DOI:10.1029/2006WR005467.

Mirus, B.B., B.A. Ebel, K. Loague, and B.C. Wemple. 2007. Simulated effect of a forest road on near-surface hydrologic response: Redux. *Earth Surface Processes and Landforms*, 32(1), 126–142.

Mirus, B.B., K. Loague, J.E. VanderKwaak, S.K. Kampf, S.J. Burges. 2009. A hypothetical reality of Tarrawarra-like hydrologic response. *Hydrological Processes*, 23(7), 1093–1103.

Newman, B.D., A.R. Campbell, and B.P. Wilcox. 1998. Lateral subsurface flow pathways in a semiarid ponderosa pine hillslope. *Water Resources Research*, 34, 3485–3496.

Nimmo, J.R. 2012. Preferential flow occurs in unsaturated conditions. *Hydrological Processes*, 26, 786–789.

Onda, Y., Y. Komatsu, M. Tsujimura, and J. Fujihara. 2001. The role of subsurface runoff through bedrock on storm flow generation. *Hydrological Processes*, 15, 1693–1706.

Rakovec, O., R. Kumar, S. Attinger, and L. Samaniego. 2016. Improving the realism of hydrologic model functioning through multivariate parameter estimation. *Water Resources Research*, 52, 7779–7792.

Saito, H., J. Šimůnek, and B.P. Mohanty. 2006. Numerical analysis of coupled water, vapor, and heat transport in the vadose zone. *Vadose Zone Journal*, 5, 784–800.

Schulz, K., R. Seppelt, E. Zehe, H.J. Vogel, and S. Attinger. 2006. Importance of spatial structures in advancing hydrological sciences, *Water Resources Research*, 42, W03S03, doi:10.1029/2005WR004301.

Scanlon, B.R., M. Christman, R. Reedy, I. Porro, J. Šimůnek, and G. Flerchinger. 2002. Intercode comparisons for simulating water balance of surficial sediments in semiarid regions. *Water Resources Research*, doi:10.1029/2001WR001233.

Salve, R., D.M. Rempe, and W.E. Dietrich. 2012. Rain, rock moisture dynamics, and the rapid response of perched groundwater in weathered, fractured argillite underlying a steep hillslope. *Water Resources Research*, 48, 1–25.

Sidle, R., S. Noguchi, Y. Tsuboyama, and K. Laursen., 2001. A conceptual model of preferential flow systems in forested hillslopes: evidence of self-organization. *Hydrological Processes*, 15, 1675–1692.

Šimůnek, J., N.J. Jarvis, M.T. van Genuchten, and A. Gardenas. 2003. Review and comparison of models for describing nonequilibrium and preferential flow and transport in the vadose zone. *Journal of Hydrology*, 272, 14–35.

925 Šimůnek, J., M.T. van Genuchten, and M. Sejna. 2006. The HYDRUS Software Package for
926 Simulating Two- and Three-dimensional Movement of Water, Heat, and Multiple
927 Solutes in Variably-Saturated Media: Technical Manual. Version 1.0. PC-Progress,
928 Prague, Czech Republic.
929 Šimůnek, J., van Genuchten, M.Th., Sejna, M. 2016. Recent developments and applications
930 of the HYDRUS computer software packages. *Vadose Zone Journal*. 15,
931 http://dx.doi.org/10.2136/vzj2016.04.0033.
932 Sivakumar, B. 2004. Dominant processes concept in hydrology: moving forward.
933 *Hydrological Processes*,18, 2349–2353.
934 Todd, M.S., P.R. Jeff, and M.H. George. 2000. Shallow subsurface storm flow in a forested
935 headwater catchment: Observations and modeling using a modified Topmodel. *Water*
936 *Resources Research*, 36(9), 2575–2586.
937 Tromp-van Meerveld, I., and M. Weiler. 2008. Hillslope dynamics modeled with increasing
938 complexity. *Journal of Hydrology*, 361, 24–40. DOI: 10.1029/2007WR006299.
939 Tromp-van Meerveld, H.J. and J.J. McDonnell. 2006. Threshold relations in subsurface
940 stormflow 1. A 147 storm analysis of the Panola hillslope. *Water Resources Research*,
941 42, W02410, doi:10.1029/2004WR003778.
942 Tromp-van Meerveld, H.J., N.E. Peters, J.J. McDonnell. 2007. Effect of bedrock permeability
943 on subsurface stormflow and the water balance of a trenched hillslope at the Panola
944 Mountain Research Watershed, Georgia, USA. *Hydrological Processes*, 21, 750–769.
945 Twarakavi, N.K.C., Šimůnek, J., Seo, H.S. 2008. Evaluating interactions between
946 groundwater and vadose zone using HYDRUS-based flow package for MODFLOW.
947 *Vadose Zone Journal*, 7, 757–768.
948 Vereecken, H., J.A. Huisman, H.J. Hendricks Franssen, N. Brggemann, H.R. Bogena, S.
949 Kollet, M. Javaux, J. van der Kruk, and J. Vanderborght. 2015. Soil hydrology: Recent
950 methodological advances, challenges, and perspectives. *Water Resources Research*, 51,
951 2616–2633.
952 van Genuchten, M.T. 1980. A closed-form equation for predicting the hydraulic conductivity
953 of unsaturated soils. *Soil Science Society of America Journal*, 44, 892–898.
954 van Genuchten, M.T., F.J. Leij, and S.R. Yates. 1991. The RETC code for quantifying the
955 hydraulic functions of unsaturated Soils. Ver. 1.0 EPA Rep. 600/2-91/065. U.S. Salinity
956 Lab., USDA-ARS, Riverside, CA.
957 Vogel, H.-J., and K. Roth. 2003. Moving through scales of flow and transport in soil. *Journal*
958 *of Hydrology*, 272, 95–106.

Weiler, M., and J.J. McDonnell. 2004. Virtual experiments: a new approach for improving process conceptualization in hillslope hydrology. *Journal of Hydrology*, 285, 3–18.

Whipkey, R.Z. 1965. Subsurface stormflow from forested slopes. *Bulletin-International Association of Scientific Hydrology*, 10, 74–85.

Zepp, H., J.L. Tang, and B. Zhang. 2005. A methodological framework for a multiscale study on hydrological processes and soil erosion in subtropical SE China. Pedosphere. 15, 695–706.

Zhao, Y., S. Peth, R. Horn, J. Krümmelbein, B. Ketzer, Y.Z. Gao, J. Doerner, C. Bernhofer, and X.H. Peng. 2010. Modelling grazing effects on coupled water and heat fluxes in Inner Mongolia grassland. *Soil and Tillage Research*, 109, 75–86.

Zhao, Y., J. Tang, C. Graham, Q. Zhu, K. Takagi, and H. Lin. 2012. Hydropedology in the ridge and valley: soil moisture patterns and preferential flow dynamics in two contrasting landscapes. In: Lin, Henry (Ed.), Hydropedology: Synergistic Integration of Soil Science and Hydrology. Academic Press.

Table 1 Soil and landscape features displayed for the s74, s54, s51, and s15 monitoring sites in the Shale Hills catchment of Pennsylvania.

| Soil series | Site number | Landform position | Slope/% | Soil horizon | Sensor depth/cm | Depth to bedrock/cm | Rock fragment/% | Soil texture |
|---|---|---|---|---|---|---|---|---|
| Weikert | 74 | Nearly planar upslope | 23.8 | Oe-A | 5 | 22 | | |
| | | | | A | 8 | | 0 | Silt loam |
| | | | | A-CR | 10 | | 60 | Silt loam |
| | | | | CR | 17 | | 90 | Silt loam |
| | | | | R | 37 | | | |
| Rushtown | 53 | Swale, upslope | 38.4 | A | 10 | >150 | 5 | Silt loam |
| | | | | Bw1 | 22 | | 5 | Silt loam |
| | | | | Bw2 | 44 | | 5 | Silt loam |
| | | | | Bw3 | 73 | | 5 | Silty clay loam |
| | | | | C | 123 | | 80 | |
| Rushtown | 51 | Swale, midslope | 13.1 | Oe-A | 5 | >300 | | |
| | | | | A | 8 | | 5 | Silt loam |
| | | | | A-Bw1 | 12 | | 5 | Silt loam |
| | | | | Bw1 | 15 | | 5 | Silt loam |
| | | | | Bw2 | 22 | | 5 | Silt loam |
| | | | | Bw3 | 40 | | 5 | Silty clay loam |
| | | | | BC | 68 | | 50 | Silty clay loam |
| | | | | BC-C1 | 92 | | 50 | Silty clay loam |
| | | | | C1 | 122 | | 80 | |
| | | | | C2 | 162 | | 80 | |
| Ernest | 15 | Valley floor | 6.6 | A | 13 | > 300 | 0 | Silt loam |
| | | | | AE-Bw | 20 | | 0 | Silt loam |
| | | | | Bt | 41 | | 0 | Silty clay |
| | | | | Bt-C2 | 52 | | 0 | Silty clay |
| | | | | C2 | 72 | | 80(soft) | Sandy loam |
| | | | | C2-C3 | 85 | | 0 | Clay |
| | | | | C4 | 109 | | 90 (soft) | Sandy loam |

Table 2 Hydraulic parameters for the different monitoring sites: (a) Van Genuchten-Mualem parameters obtained from inverse modeling with field data, (b) dual-porosity model parameters obtained obtained from inverse modeling with field data (immobile water parameters indicated by subscript im, and mobile regions indicated by subscript mo). $a_w$ is a first-order mass transfer coefficient.

| Site | Soil depth (cm) | (a) Van Genuchten-Mualem Model | | | | | | (b) Dual-Porosity Model | | | | |
|---|---|---|---|---|---|---|---|---|---|---|---|---|
| | | $\theta_r$ ($cm^3cm^{-3}$) | $\theta_s$ ($cm^3cm^{-3}$) | $\alpha$ ($cm^{-1}$) | $n$ (-) | $K_s(K_v/K_h)$ (cm $d^{-1}$) | $l$ (-) | $\theta r_{mo}$ ($cm^3cm^{-3}$) | $\theta s_{mo}$ ($cm^3cm^{-3}$) | $\theta r_{im}$ ($cm^3cm^{-3}$) | $\theta s_{im}$ ($cm^3cm^{-3}$) | $a_w$ ($cm^{-1}d^{-1}$) |
| 74 | 0-5 | 0.020 | 0.260 | 0.247 | 1.523 | 316/80 | 0.5 | 0 | 0.160 | 0.020 | 0.100 | 1.839E-04 |
| | 5-15 | 0.000 | 0.290 | 0.036 | 1.714 | 3003/265 | 0.5 | 0 | 0.190 | 0.000 | 0.100 | 1.098E-03 |
| | 15-30 | 0.030 | 0.250 | 0.020 | 1.547 | 301/320 | 0.5 | 0 | 0.100 | 0.030 | 0.150 | 7.198E-01 |
| | 30-76 | 0.040 | 0.400 | 0.022 | 1.473 | 109/560 | 0.5 | 0 | 0.150 | 0.040 | 0.250 | 1.934E-04 |
| 53 | 0-10 | 0.000 | 0.440 | 0.007 | 2.277 | 1123/159 | 0.5 | 0 | 0.350 | 0.000 | 0.090 | 5.953E-04 |
| | 10-40 | 0.040 | 0.380 | 0.008 | 2.089 | 5/245 | 0.5 | 0 | 0.300 | 0.040 | 0.080 | 2.066E-05 |
| | 40-80 | 0.040 | 0.330 | 0.021 | 1.594 | 293/370 | 0.5 | 0 | 0.180 | 0.040 | 0.150 | 5.579E-03 |
| | 80-149 | 0.010 | 0.260 | 0.006 | 1.846 | 318/690 | 0.5 | 0 | 0.150 | 0.010 | 0.110 | 5.930E-04 |
| 51 | 0-10 | 0.030 | 0.400 | 0.080 | 1.580 | 150/116 | 0.5 | 0 | 0.360 | 0.030 | 0.040 | 2.000E-04 |
| | 10-30 | 0.050 | 0.450 | 0.011 | 3.461 | 602/270 | 0.5 | 0 | 0.350 | 0.000 | 0.150 | 9.301E-03 |
| | 30-50 | 0.030 | 0.330 | 0.012 | 2.278 | 144/2100 | 0.5 | 0 | 0.200 | 0.000 | 0.160 | 2.623E-03 |
| | 50-100 | 0.050 | 0.300 | 0.037 | 1.801 | 299/410 | 0.5 | 0 | 0.150 | 0.080 | 0.120 | 2.056E-03 |
| | 100-236 | 0.030 | 0.300 | 0.009 | 2.095 | 2/450 | 0.5 | 0 | 0.160 | 0.050 | 0.140 | 6.651E-03 |
| 15 | 0-20<br>20-52 | 0.050 | 0.450 | 0.023 | 2.228 | 27/170 | 0.5 | 0 | 0.390 | 0.050 | 0.060 | 5.390E-04 |
| | 52-83 | 0.080 | 0.430 | 0.013 | 1.962 | 2485/230 | 0.5 | 0 | 0.330 | 0.080 | 0.100 | 1.134E-05 |
| | 83-91 | 0.120 | 0.420 | 0.012 | 1.716 | 273/320 | 0.5 | 0 | 0.290 | 0.100 | 0.150 | 2.024E-04 |
| | 91-260 | 0.100 | 0.370 | 0.100 | 1.450 | 100/310 | 0.5 | 0 | 0.250 | 0.100 | 0.120 | 2.000E-04 |
| | 0-10 | 0.130 | 0.350 | 0.014 | 1.355 | 57/130 | 0.5 | 0 | 0.200 | 0.100 | 0.180 | 2.038E-04 |

Table 3 Nash–Sutcliffe efficiency (*NSE*) values and root mean square errors (*RMSE*) of the 1D, 2D, and 3D simulation modeling approaches during the one hydrological year 2007 at the s74 and s15 monitoring sites as used in the dual-porosity model (DP), fractured bedrock (FB), and Isotropy $K_s$. Comparisons included the corresponding 3D simulations of single-porosity model (VG), impermeable bedrock (IB), and anisotropy $K_s$ (Ani).

| Site | Soil depth (cm) | Simulation by Dual-porosity model (DP), fractured bedrock (FB) and Isotropy Ks | | | | | | Comparisons | | | | | |
|---|---|---|---|---|---|---|---|---|---|---|---|---|---|
| | | *NSE* | | | *RMSE* | | | *NSE* | | | *RMSE* | | |
| | | 1D | 2D | 3D | 1D | 2D | 3D | VG | BI | Ani | VG | BI | Ani |
| 74 | 5 | -0.319 | -0.153 | **0.722** | 0.045 | 0.042 | 0.021 | -0.582 | **0.705** | -0.820 | 0.050 | 0.021 | 0.053 |
| | 10 | 0.169 | 0.296 | **0.599** | 0.035 | 0.032 | 0.024 | 0.329 | **0.737** | 0.036 | 0.031 | 0.020 | 0.038 |
| | 17 | -2.047 | 0.423 | **0.734** | 0.068 | 0.030 | 0.020 | 0.456 | **0.646** | -2.223 | 0.029 | 0.023 | 0.070 |
| | 37 | -2.538 | -1.475 | -0.195 | 0.036 | 0.030 | 0.021 | -1.330 | -0.087 | -16.823 | 0.029 | 0.020 | 0.080 |
| 51 | 18 | -1.562 | 0.239 | 0.498 | 0.067 | 0.036 | 0.030 | -1.026 | 0.312 | -1.026 | 0.059 | 0.034 | 0.059 |
| | 40 | -0.627 | 0.191 | **0.516** | 0.042 | 0.029 | 0.023 | -1.307 | 0.439 | -1.307 | 0.050 | 0.025 | 0.050 |
| | 92 | -0.441 | -0.628 | **0.667** | 0.032 | 0.034 | 0.015 | 0.017 | 0.222 | -0.036 | 0.026 | 0.023 | 0.027 |
| | 162 | -3.790 | -2.015 | -0.676 | 0.044 | 0.035 | 0.026 | -12.558 | -3.448 | -2.874 | 0.074 | 0.043 | 0.040 |

(a)

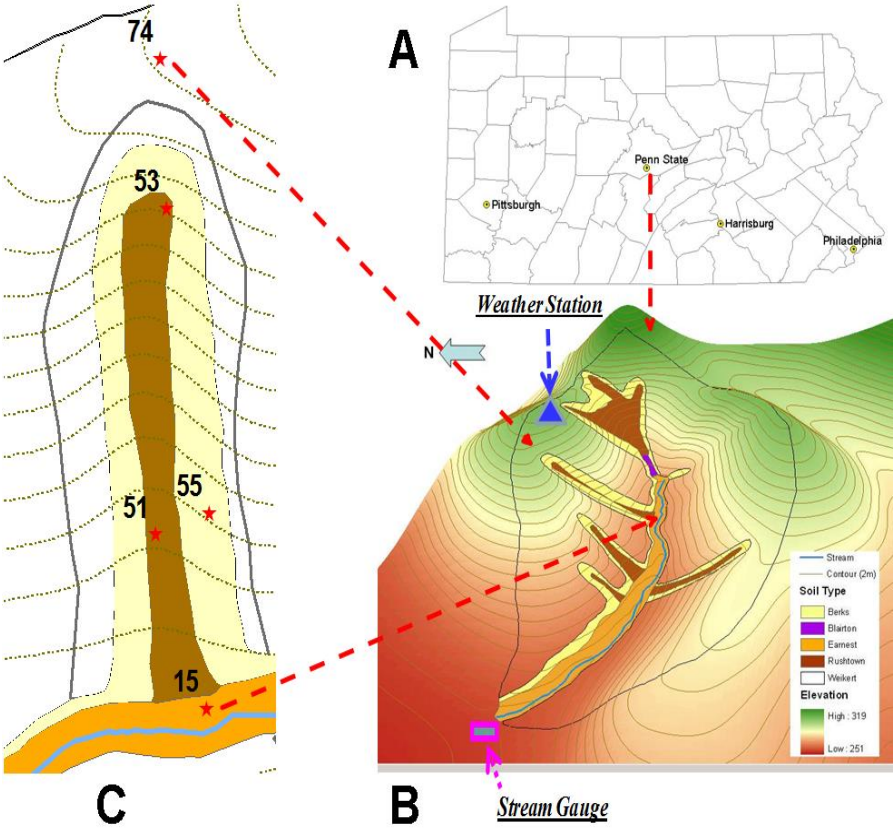


(b)

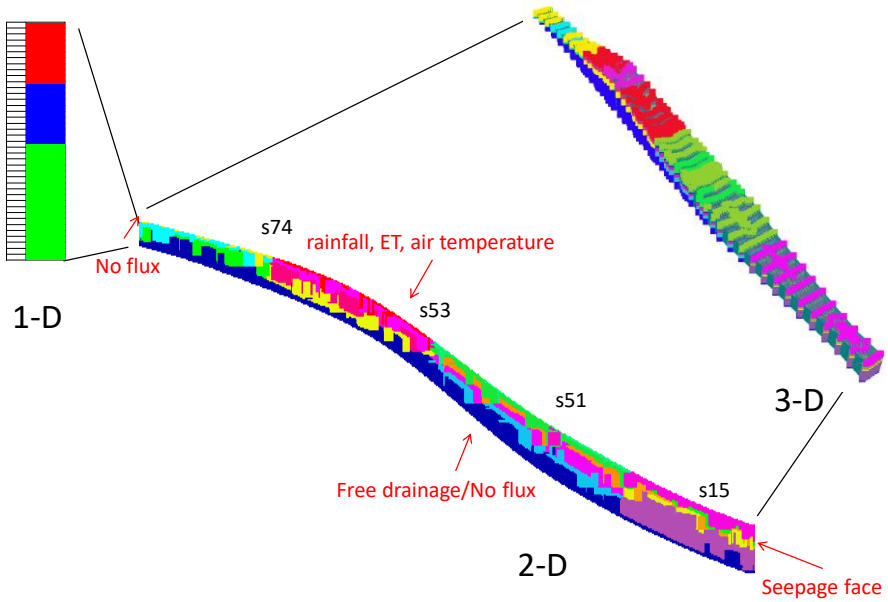


Figure 1. (a) Location (A) and shape (B) of the Shale Hills catchment, and the study hillslope (C), and (b) graphical representation of the HYDROUS-1D, -2D, and -3D simulation approaches used for the soil domain with 18 different soil materials as characterized by the different colors and the locations of the s74, s53, s51, and s15 monitoring sites with the applied boundary conditions.

(a)

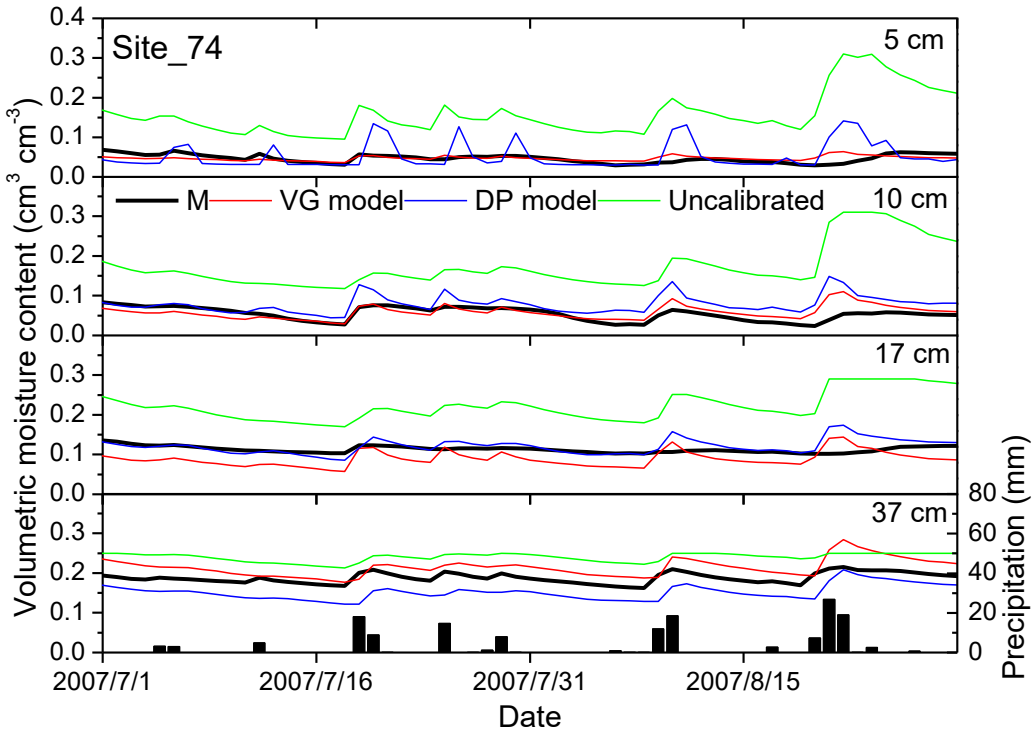


(b)

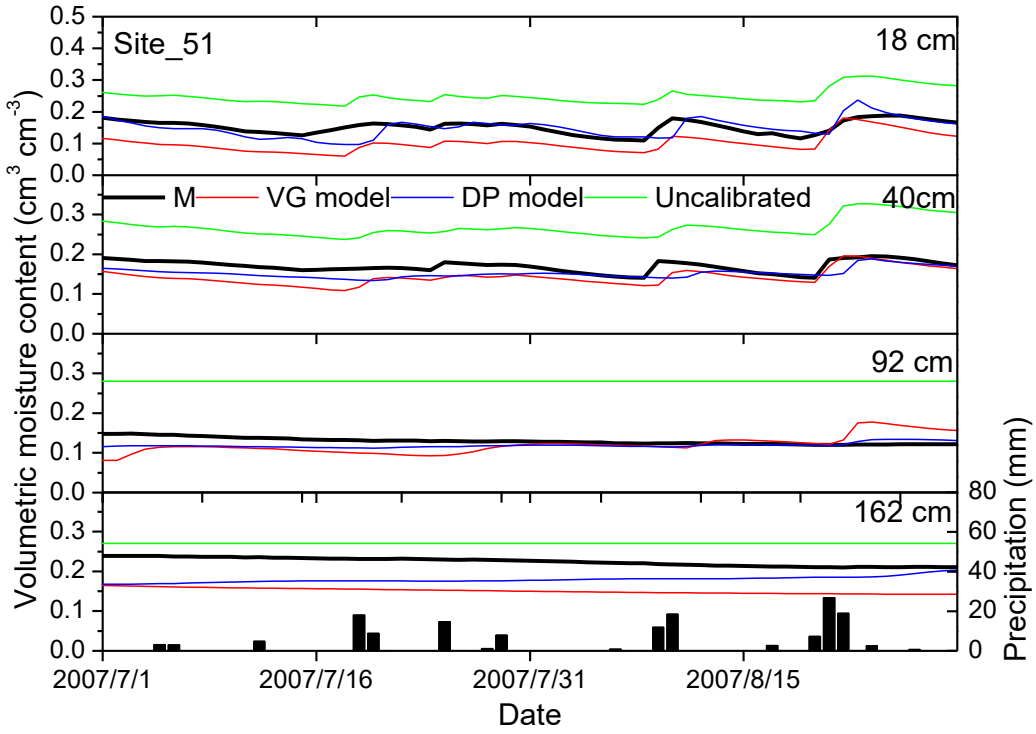


Figure 2. Comparison of the predicted and measured soil moisture values and rainfall quantities displayed over time for use in the 1D (C_1D) and 2D (C_2D) calibrations of HYDRUS at site 74 (a) and site 51 (b). The calibration results for site_53 (c) and site_15 (d) are provided in the supplement file.

(a)

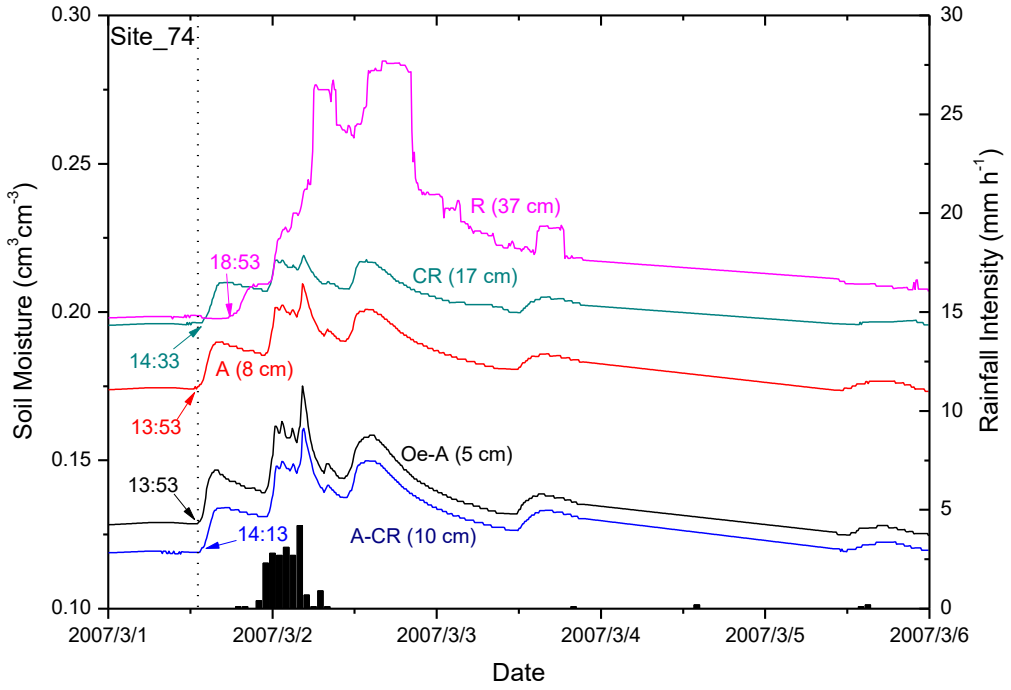


(b)

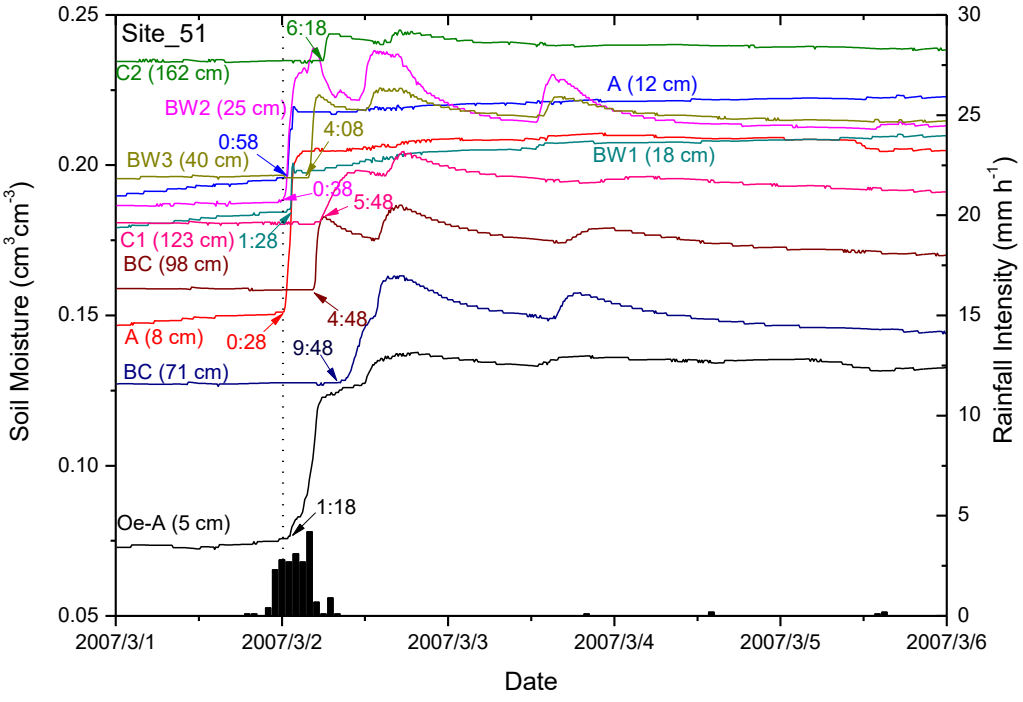


Figure 3. Volumetric soil moisture contents and rainfall intensities displayed over time during the wetter period of March 1-5, 2007 at site_74 (a) and site_51 (b). The time at which soil moisture contents started to increase following a rainfall event is indicated by bold arrows. The different colored lines identify the soil horizons with the horizon layer in capital letters and the depth of soil moisture content in parenthesis. The results for site_53 (c) and site_15 (d) are provided in the supplement file.

(a)

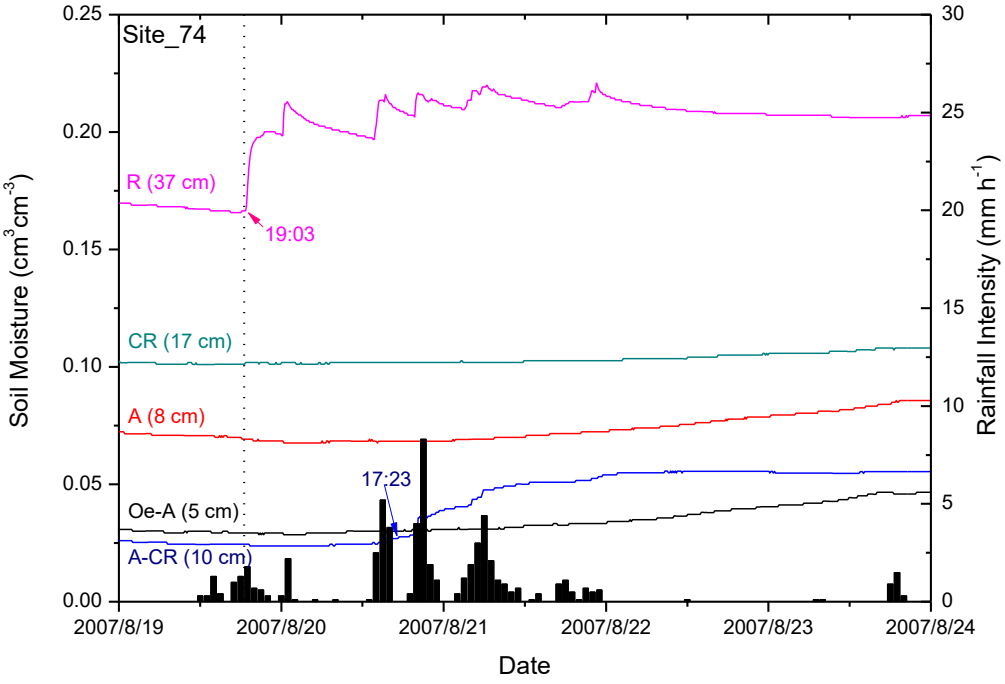


(b)

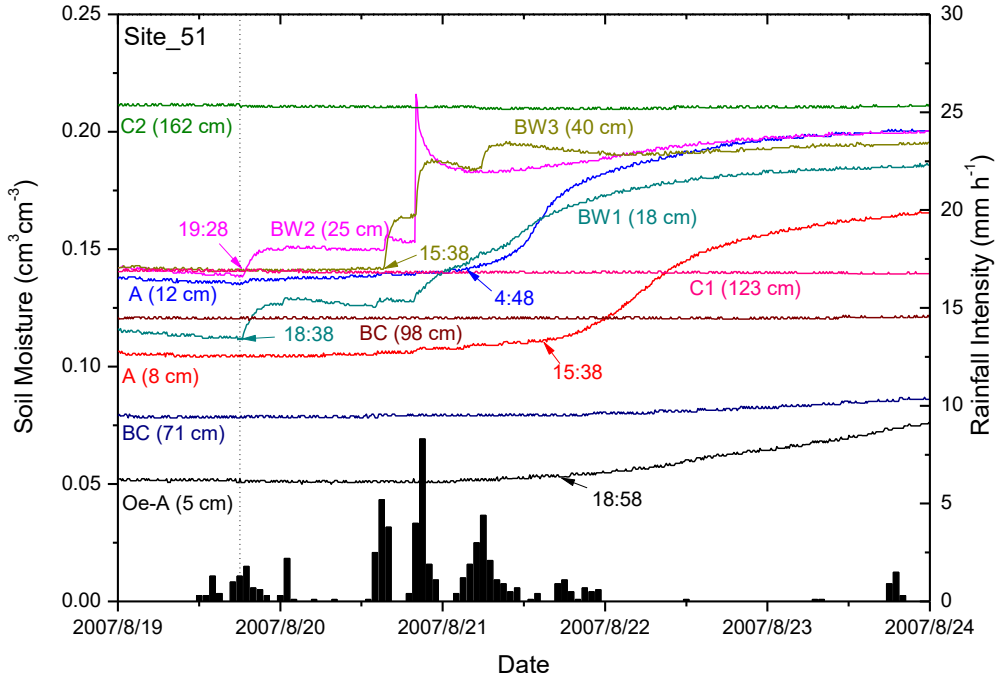


Figure 4. Volumetric soil moisture contents and rainfall intensities displayed over time during the drier period of August 19-24, 2007 at site_74 (a) and site_51 (b). The time at which soil moisture contents started to increase following a rainfall event is indicated by bold arrows. The different colored lines identify the soil horizons with the horizon layer in capital letters and the depth of soil moisture content in parenthesis. The results for site_53 (c) and site_15 (d) are provided in the supplement file.

(a)

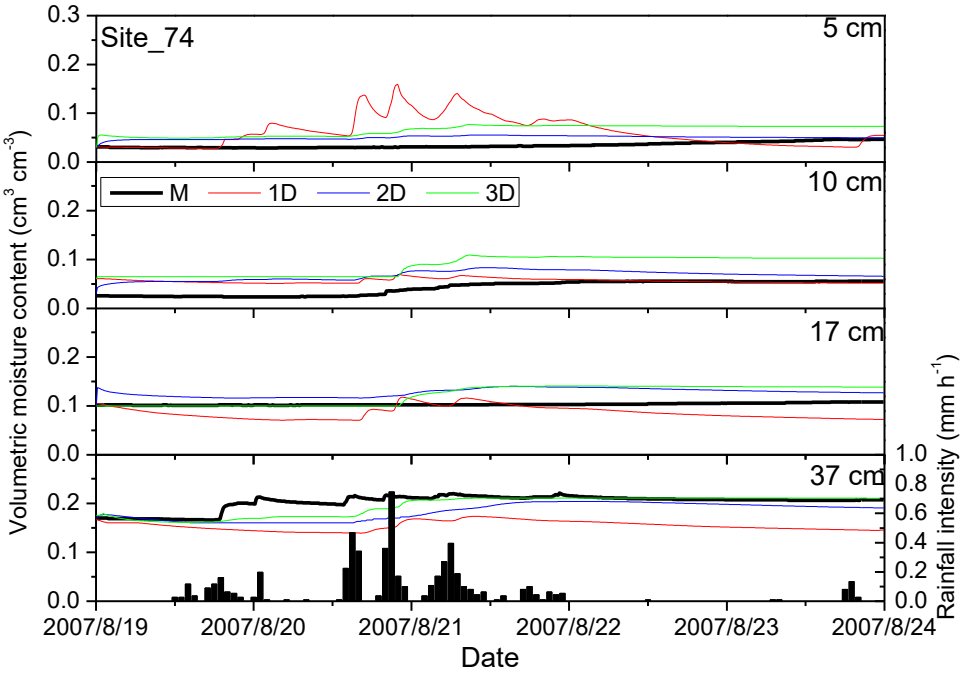


(b)

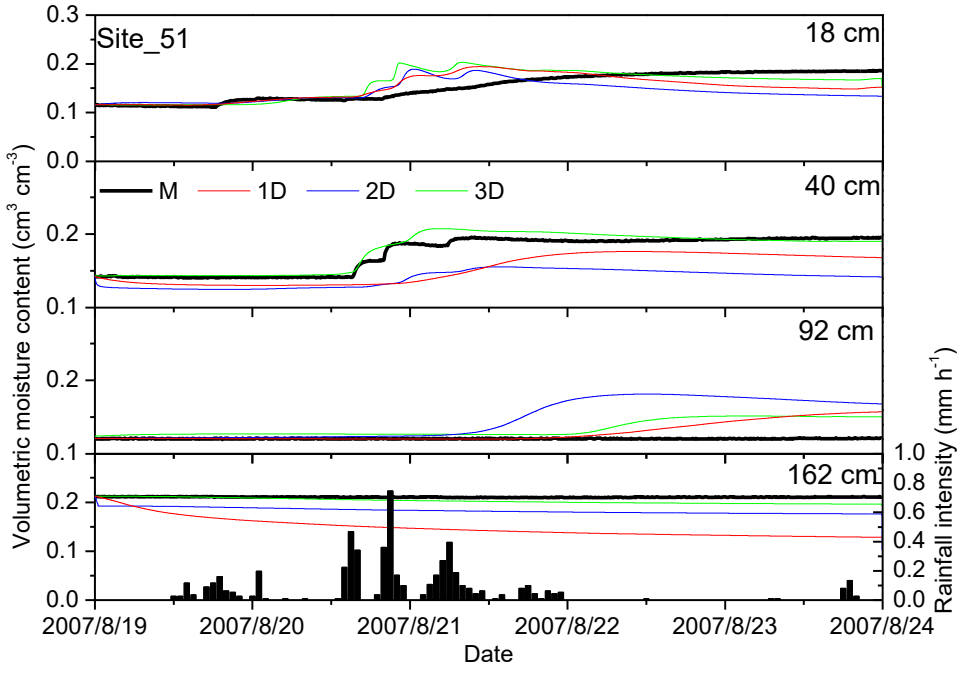


Figure 5. Predicted and measured (M) soil moisture values and rainfall intensities displayed over time during the drier period of August 19-24, 2007 at site_74 (a) and site_51 (b) by the HYDRUS-1D, -2D and -3D models. Results for site 53 (c) and site_15 (d) are provided in the supplement file.

(a)

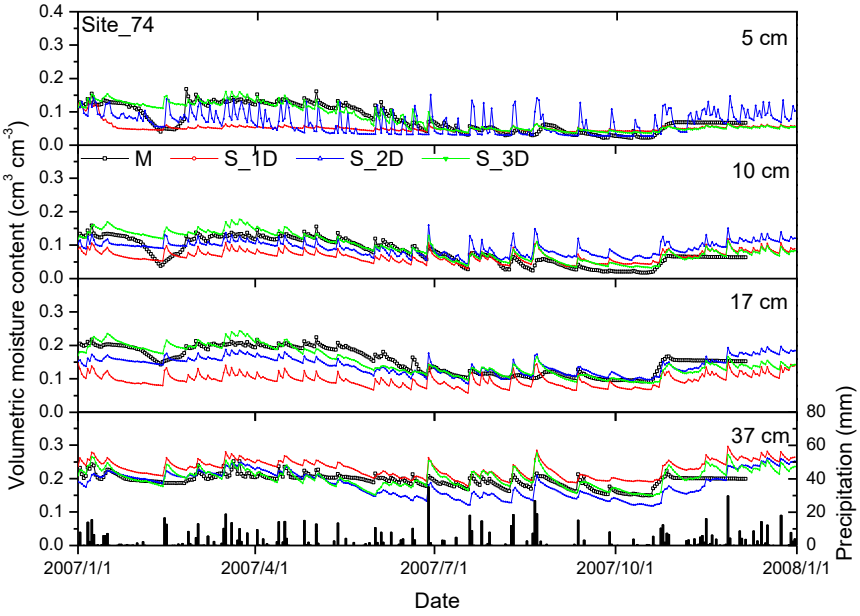


(b)

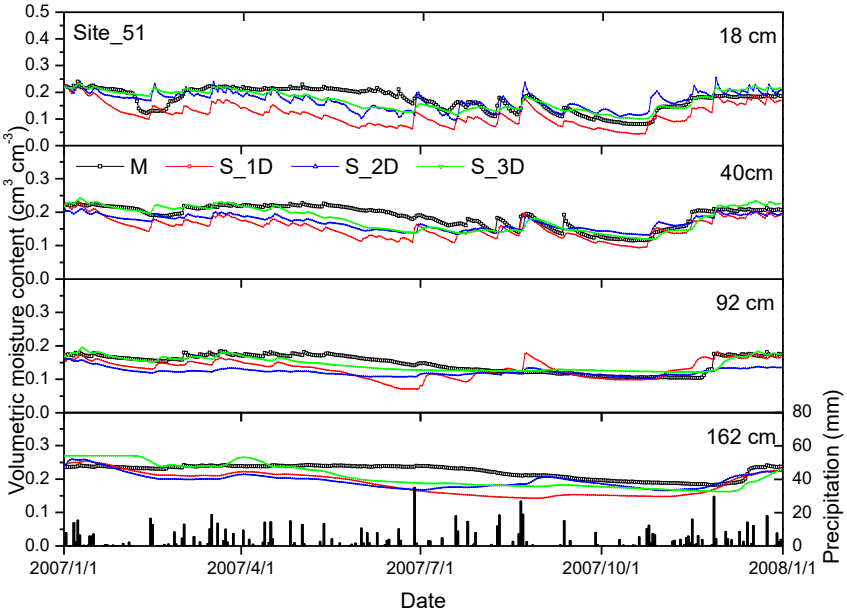


Figure 6. Predicted and measured (M) soil moisture values and rainfall intensities displayed over time in 2007 at site_74 (a) and Site_51 (b) by the HYDRUS-1D, -2D and -3D models. Results for Site_53 (c) and site_15 (d) are provided in the supplement file.

(a)

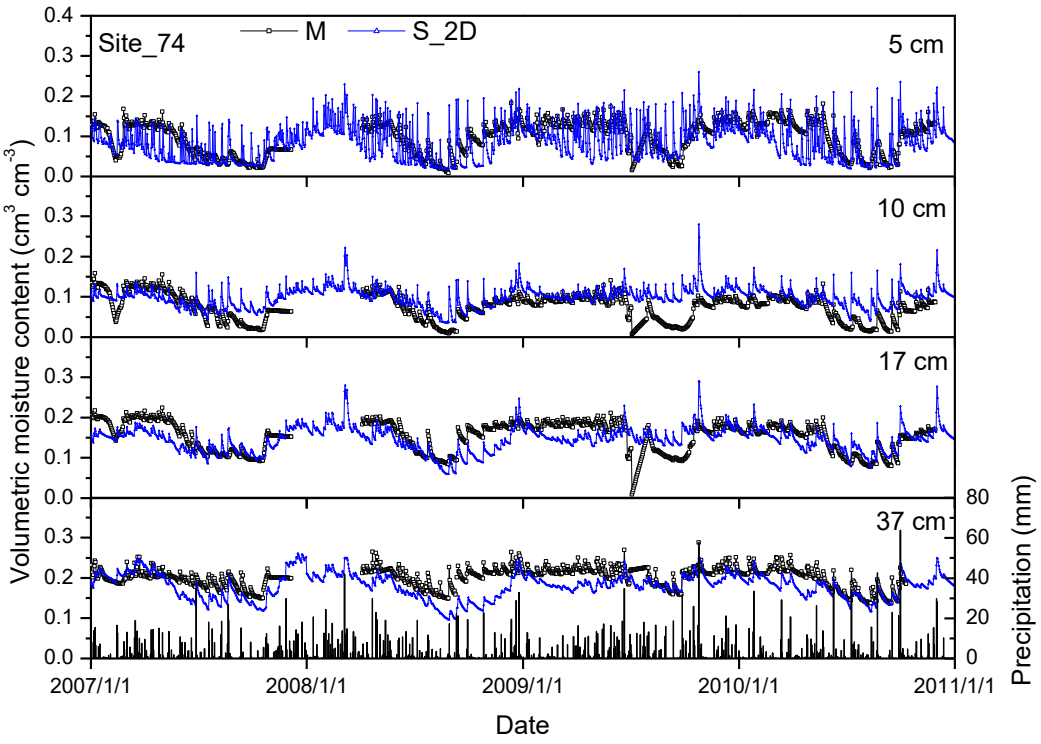


(b)

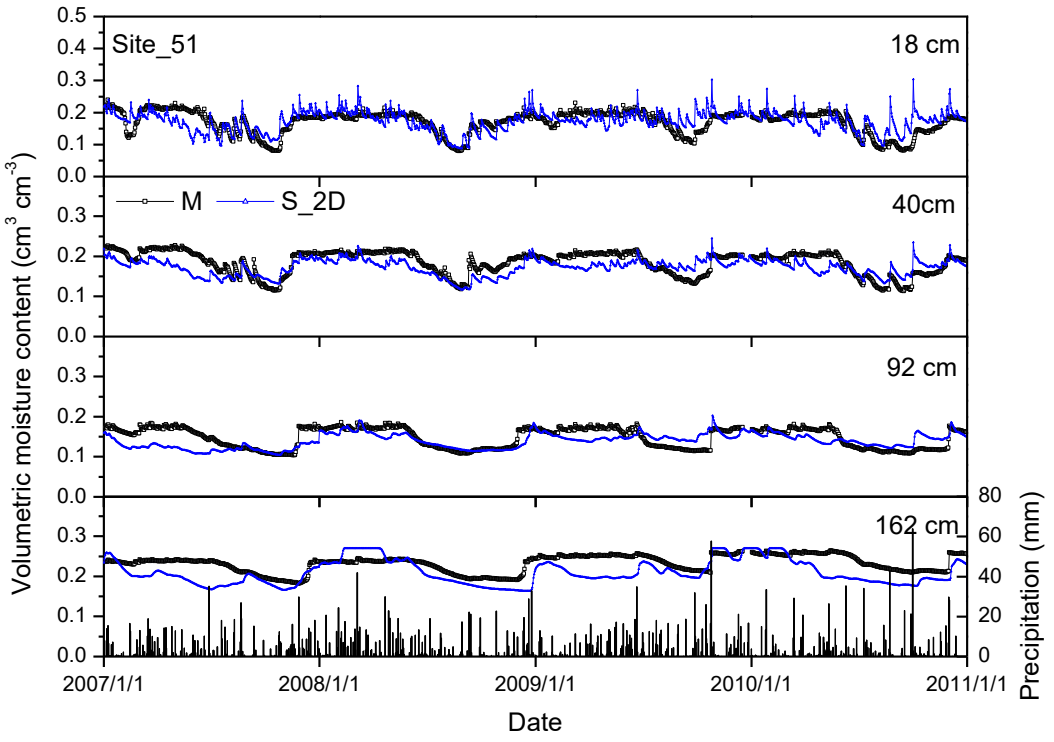


Figure 7. Predicted and measured (M) soil moisture values and rainfall intensities displayed over time in 2007-2010 for site_74 (a) and site_51 (b) by the HYDRUS- 2D model. The results for site_53 (c) and site_15 (d) are provided in the supplement file.

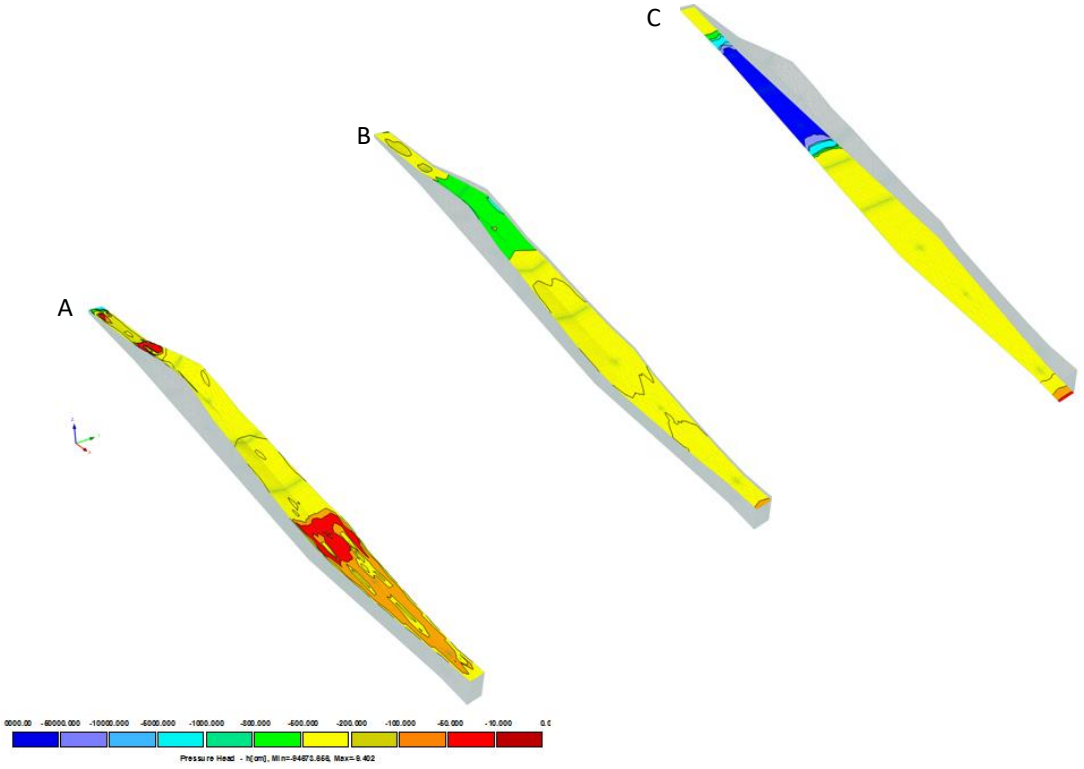


Figure 8. Spatially variable pressure head snapshots at the 0-cm topsoil (A), the 40-cm subsoil (B), and the soil/bedrock interface (C) that were simulated by HYDRUS for August 20, 2007.

(a)

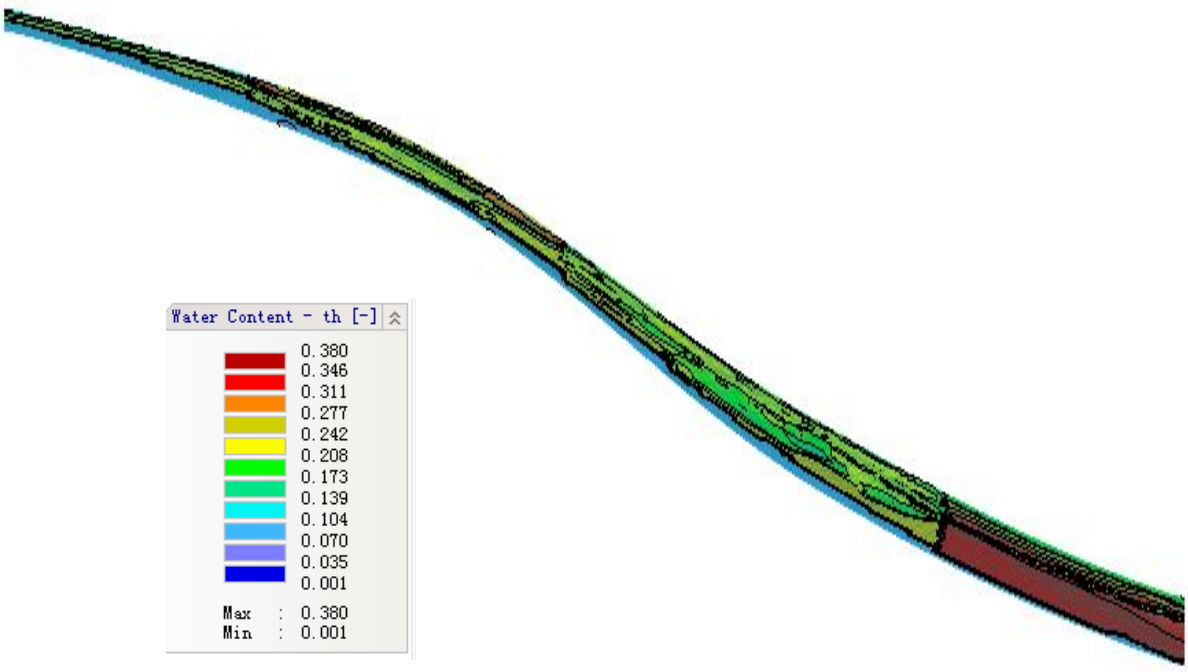


(b)

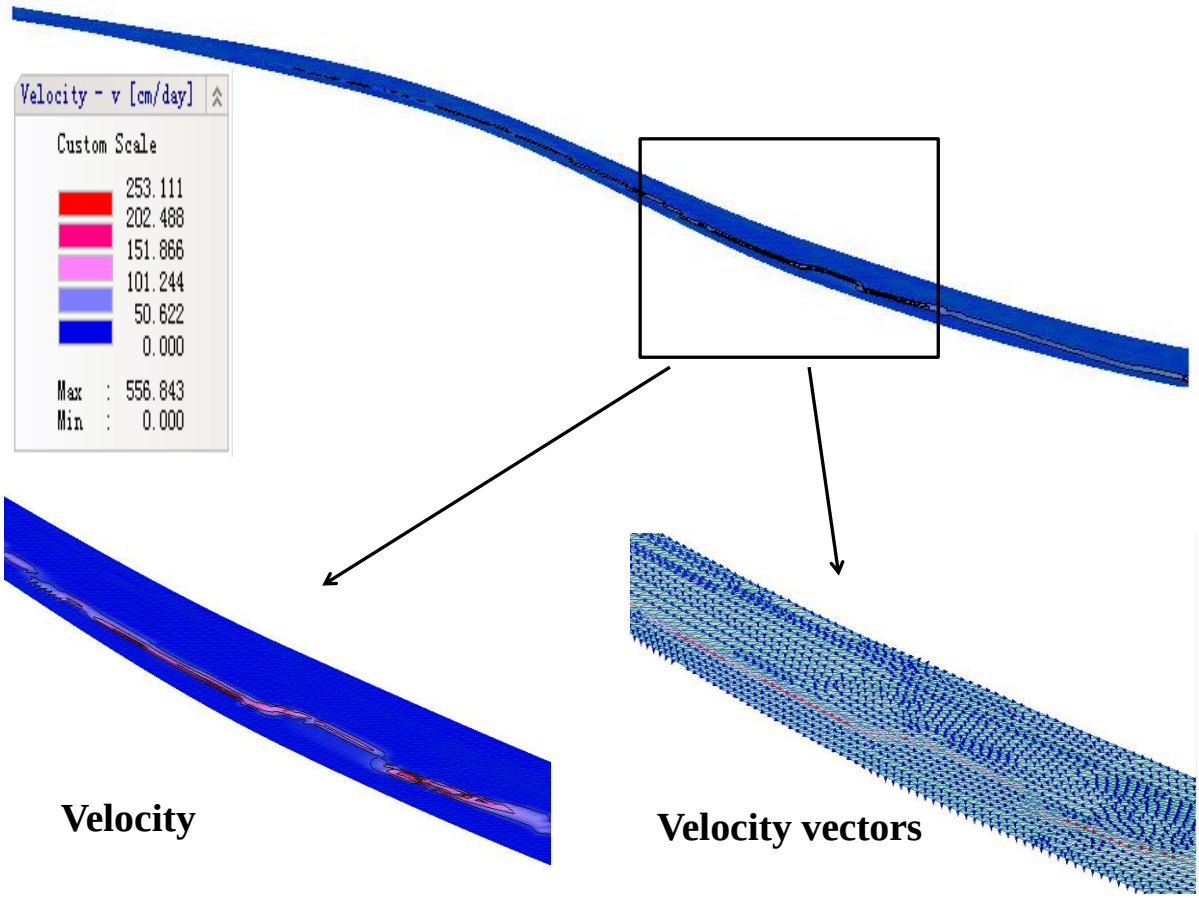


Figure 9. The 2D-distribution of (a) soil moisture content values and (b) water flux velocities displayed for August 20, 2007.

(a)

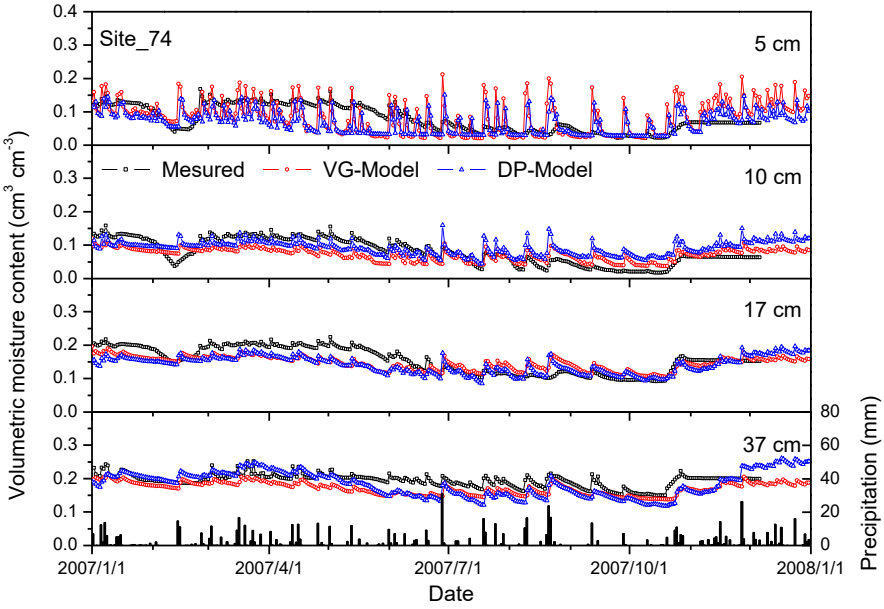


(b)

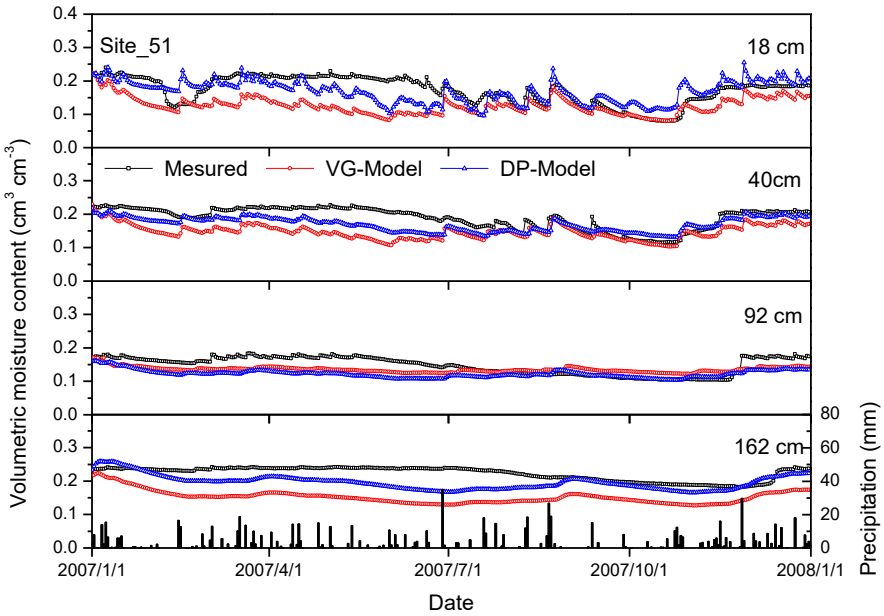


Figure 10. Comparisons between measured and predicted soil moisture values over time in 2007 for the uniform flow model (VG) and the dual porosity model (DP) at site 74 (a) and site 51 (b) by the HYDRUS-2D model.

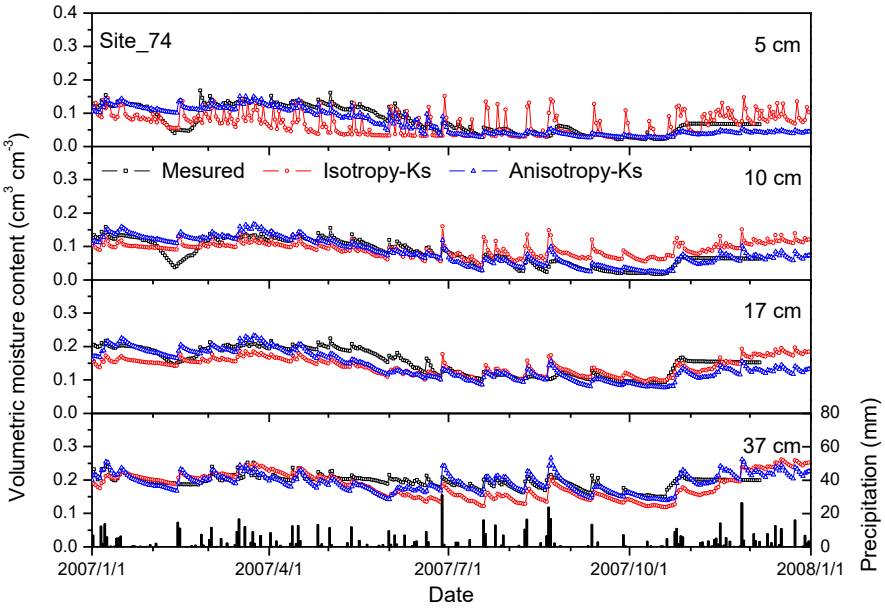


(b)

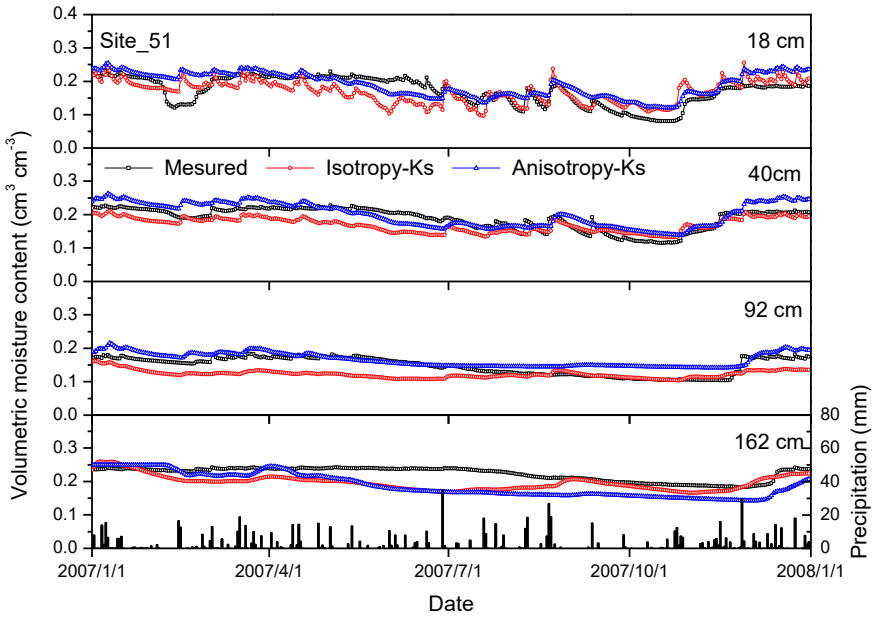


Figure 11. Comparisons between measured and predicted soil moisture values displayed over time in 2007 for isotropy-Ks and anisotropy-Ks at site 74 (a) and site 51 (b) by the HYDRUS-2D model.

(a)

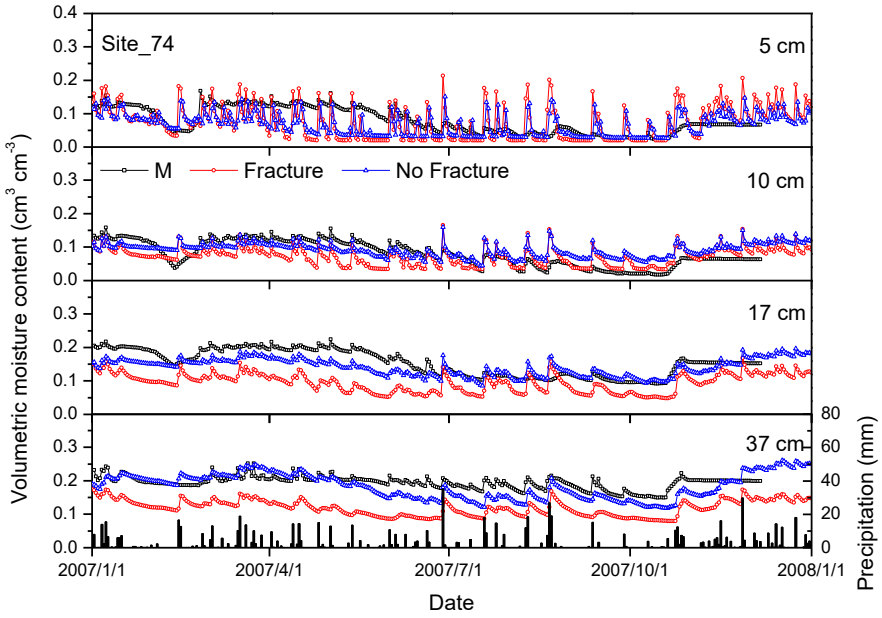


(b)

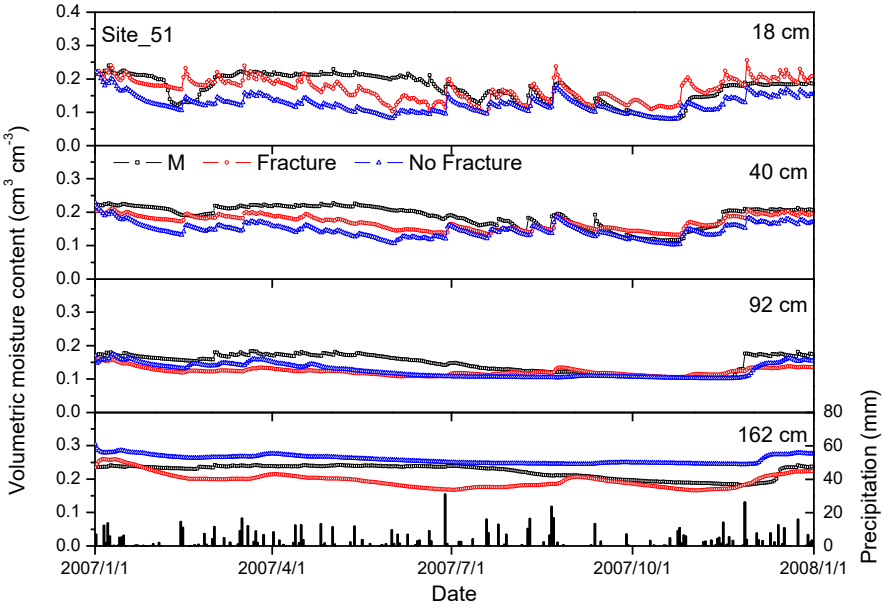


Figure 12. Comparisons between measured and predicted soil moisture values displayed over time in 2007 for fracture and no fracture bedrock structures for site 74 (a) and site 51 (b) by the HYDRUS-2D model.

(a)

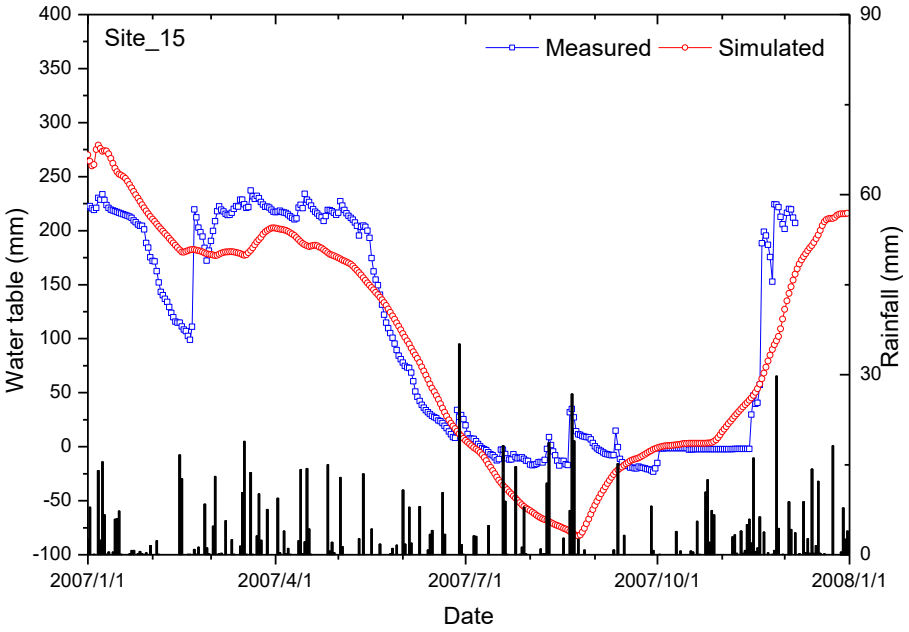


(b)

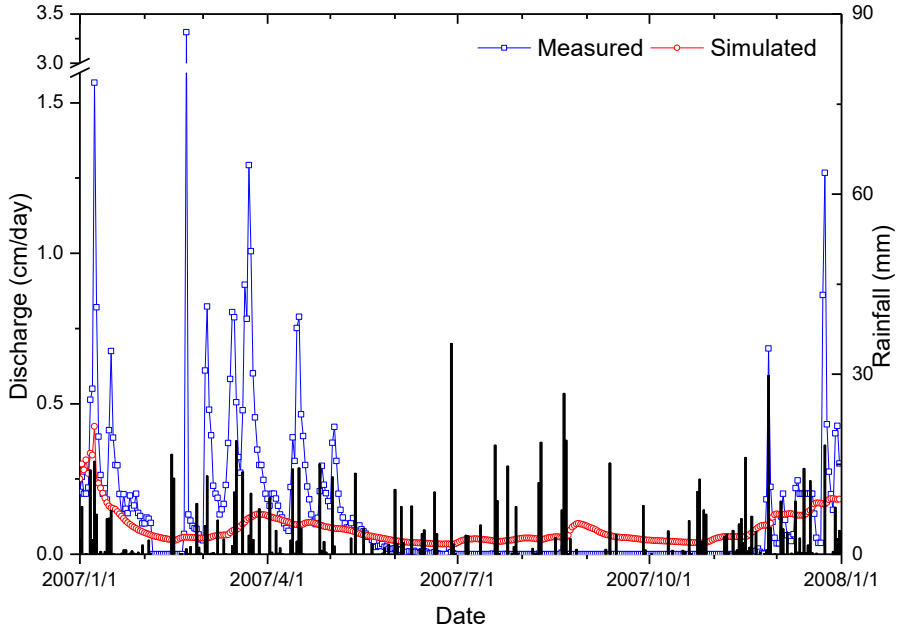


Figure 13. Comparisons between measured and simulated water tables for site 15 (a) and the measured discharge at the outlet of the catchment and simulated discharge for the sub-catchment evaluated during this study (b) with rainfall quantity distribution as a reference.

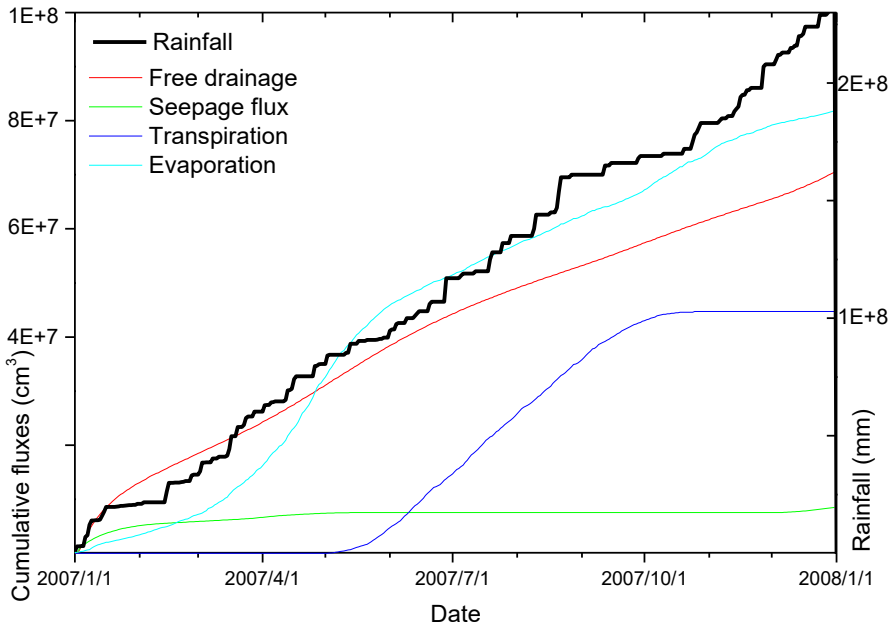


Figure 14. Simulated water balances displayed over time for the sub-catchment in 2007 comparing cumulative rainfall with cumulative flux estimations of free drainage, seepage flux, transpiration, and evaporation.

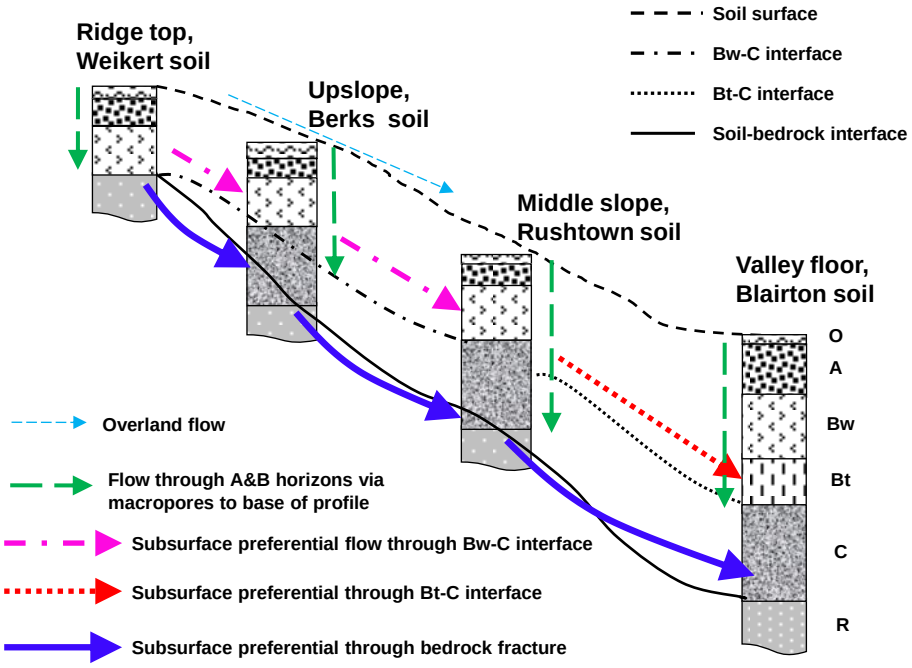


Figure 15. Conceptual diagram showing several potential subsurface preferential flow pathways along a hillslope in the Shale Hills catchment. The soil series and soil horizons are indicated for each landscape position, which is referenced to Table 1.